Reliability Engineering and System Safety 238 (2023) 109474

Contents lists available at ScienceDirect

Reliability Engineering and System Safety

journal homepage: www.elsevier.com/locate/ress

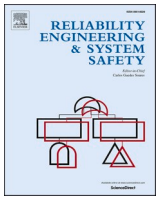

A receptor-centric decision support system for the mitigation of nuclear power atmospheric release incidents

Arshad Mohamed Ali , Konstantinos E Kakosimos *

Department of Chemical Engineering and Mary Kay O'Connor Process Safety Center Qatar, Texas A&M University at Qatar, Qatar

ARTICLE INFO

Original content: Processed Simulation Data used in generating tables and figures in Manuscript (Original data)

Keywords:
Decision support system
Hypothetical nuclear accident
Receptor-centric
Qatar

ABSTRACT

The history of incidents involving nuclear power plants underscores the imperative for robust consequence assessment and countermeasure plans. Additionally, the recent energy crisis has reaffirmed the enduring necessity of nuclear energy. While a host of assessments, planning, and response fundamentals exist, the literature lacks specific directives for their implementation. Notably, despite a wealth of studies employing the entire suite of available tools (i.e., source release, atmospheric dispersion and deposition, food contamination, and human exposure) for hypothetical or actual cases, the majority tend to focus on the source and fate of nucleoids. Given these circumstances, we propose a receptor-centric and data-driven framework to guide the selection and evaluation of such planning. This framework, which utilizes time-dependent source terms and the JRODOS system, is exemplified within a region home to multiple nuclear plants. Significantly, this new approach proved more robust than traditional wind-rose and worst-case methodologies in capturing a broader spectrum of potential outcomes. Though it was possible to prioritize and validate certain countermeasures, such as sheltering and food restrictions, using the innovative visualization methods within the framework, we identified several limitations. These weaknesses, along with potential avenues for future research, are discussed in this study, contributing valuable insights to this crucial field.

1. Introduction

Several nuclear accidents with varying consequences have occurred worldwide since 1952, with the Chernobyl, Three-mile island, and Fukushima Daiichi accidents being the most widely known [1,2]. These accidents, especially Fukushima Daiichi, have highlighted the importance of an effective and versatile emergency response plan (ERP) to mitigate the consequences of a nuclear accident [3]. The necessity of robust consequence assessment and countermeasure plans for an effective Emergency Response Plan (ERP) is emphasized by FEMA [4]. Key aspects of planning include 'community-based planning' which caters to diverse population needs and regional variances, and 'considering all hazards and threats' for flexible, scalable disaster management solutions [4]. For instance, areas with fewer car owners might require alternative evacuation strategies [4]. Equally important is the safeguarding of critical infrastructure with a systematic approach to minimize disruption [5,6]. Despite the clarity of these guidelines, their practical implementation in planning remains nebulous. However, atmospheric dispersion models and integrated Decision Support Systems (DSS) are commonly used tools in this area.

Decision Support Systems (DSS) model radionuclide pathways from source to receptors, validated largely through retrospective studies of incidents like Chernobyl and Three Mile Island, leading to systems such as JRODOS (EU), ARGOS (Worldwide), and NARAC (USA) [7–9]. Other global examples include SPEEDI (Japan) and ONERS (India) [10,11]. Rich literature exists on past disasters and exposure assessments' uncertainty and sensitivity [3,12–16]. Yet, this work focuses more on preparing for hypothetical and future incidents using DSS-like models.

Numerous studies have examined the potential impact of hypothetical accidents at specific nuclear power plants (NPP). For instance, the potential health and environmental consequences of a hypothetical accident at the UK's Sellafield nuclear plant on Norway were modeled [17,18], as were hypothetical incidents at proposed NPPs in Nigeria and Haiyang NPP in China [19–22]. These analyses, along with probabilistic risk assessments [23,24], exemplify the shift towards predictive, scenario-based ERP preparation. In particular, the emphasis was on the understanding of nuclear accident risk management, enhancing traditional Probabilistic Risk Assessment (PRA) [25] models with innovative

* Corresponding author at: PO Box 23874, Doha, Qatar, 219R Texas A&M Engineering Building, Education City.
E-mail address: k.kakosimos@qatar.tamu.edu (K.E. Kakosimos).

https://doi.org/10.1016/j.ress.2023.109474
Received 10 January 2023; Received in revised form 23 June 2023; Accepted 24 June 2023
Available online 25 June 2023

approaches. Cho et al. [24] underscored the limitations of traditional Level 2 PSA and suggested an exhaustive simulation approach that promised more comprehensive risk information, including plant responses and source term behaviors during severe accidents. This approach seemed to align with Di Maio et al. [26] proposition for a time-dependent reliability approach that accounted for aging and degradation in nuclear power plant structures [27], specifically the reinforced concrete Reactor Building. Earlier, Cho and Han [28] proposed a fresh approach to identify significant structures, systems, and components in nuclear power plants by quantifying risk importance measures, supporting risk-informed management. Similarly, Queral et al. [29] and París et al. [30] utilized the Integrated Safety Assessment (ISA) methodology, focusing on the analysis of full spectrum loss of coolant accident sequences and the Total Loss of Feedwater sequences, respectively. Studies by Rebollo et al. [31] and Song et al. [32] highlighted the importance of analyzing sequences that released large quantities of radioactive products and the need for a multi-unit probabilistic safety assessment, respectively. Taken together, these studies advocated for more comprehensive, scenario-based, and time-dependent risk assessment methods [33,34], aligning with the focus in this work.

Noteworthy, a considerable number of studies were found for NPP's in the Middle East region, possibly due to the geopolitical concerns behind the use of nuclear power [35] and the increasing number of NPPs within the region (see Fig. 1). The majority of the studies have been conducted to understand the risk to the population from the Bushehr NPP in Iran in case of releases during standard operation [36,37] and accidents [36,38–40]. Apart from Bushehr, accidents at Barakah NPP in UAE [40] and a hypothetical NPP in Iraq [41] were also studied. Interested readers can also refer to other similar studies for hypothetical nuclear accidents and their impacts on countries such as Ghana [42], China [43,44], and Malaysia [45].

A detailed analysis of the hypothetical accident studies reveals some interesting patterns: i) Most of the studies are 'plant-centric' as they center their analysis on the NPP except for a few [17,18,21]. This approach helps study the risk of proposed plants for the surrounding communities. However, this approach ignores the diversity in the various receptors (cities, industrial areas), which significantly impacts the dosage profile and criticality; ii) The majority of studies pick specific time frames i.e. specific days of the year, to simulate accidents and then extrapolate the results to analyze the disaster's impact at any time frame. While helpful to plan for the worst-case disaster, this approach leads to a non-versatile consequence assessment as they fail to account for source term and weather variations; iii) All the related studies focus only on accidents from one NPP and do not consider combining data for accidents at different NPPs; and iv) Finally, the majority of the studies use a non-time-dependent source term as part of their simulations. Thus, the most common approaches in the literature contrast with FEMA's, and other's recommendations to use 'community-based planning' and to consider all hazards and threats during the planning phase.

In the absence of a clear literature method to implement the FEMA guidelines, this study proposes a prototype DSS to incorporate these fundamental planning guidelines (outlined in Chapter 2), demonstrates it (in Chapter 3) for the assessment of the hypothetical consequences of multiple NPPs within a specific region, and discusses (in Chapter 4) the selection and efficiency of potential countermeasures. The overarching goal remains to demonstrate the utility of a receptor-centric and data-driven (explained below) prototype DSS for nuclear accidents rather than reproducing one of the detailed and exhaustive studies of accidental releases from an NPP or a multi-unit NPP [49]. To achieve the goal this study focuses on answering the following questions for a study area with some unique characteristics that will be described later:

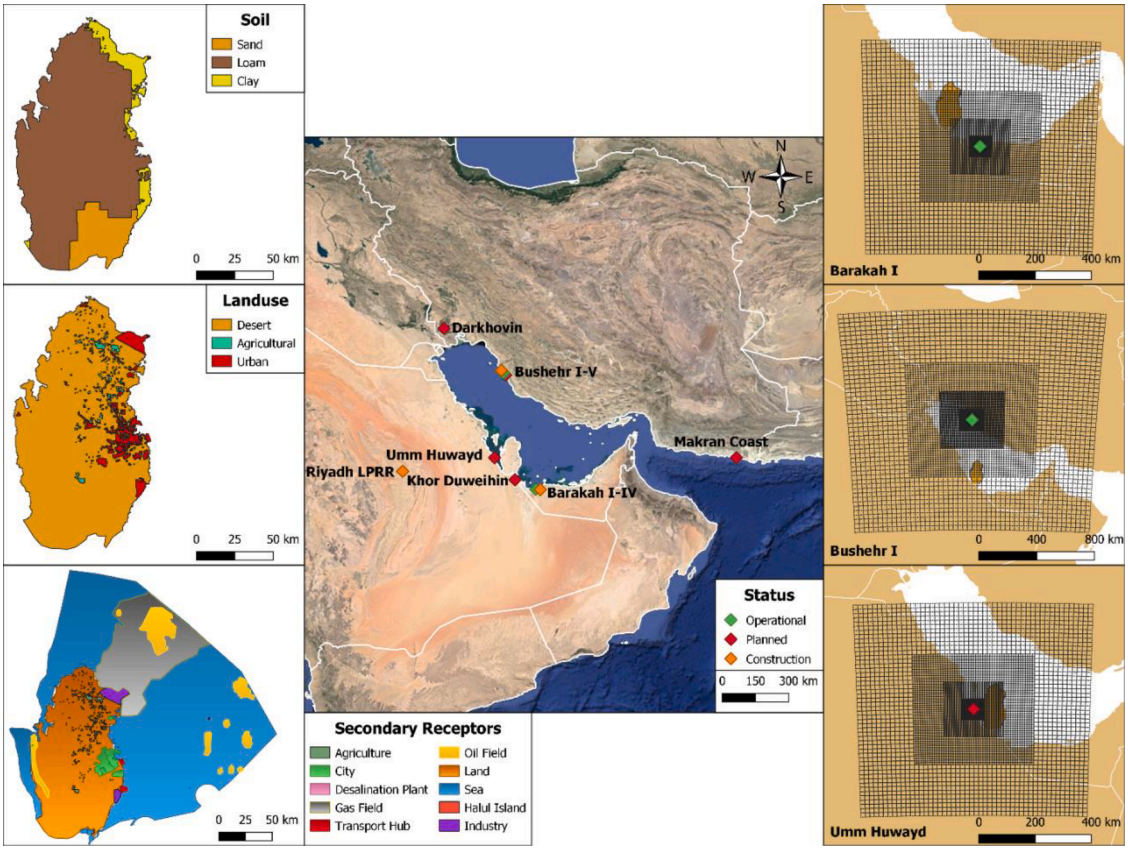

Fig. 1. Left (Top to Bottom): Soil distribution, Land use Classifications, and Secondary Receptor Subdivision Maps. Middle: Current & potential NPPs (Data from US EIA, NPR & World Nuclear Association [46–48]) Locations are taken from Google Maps and satellite imagery Right: Grid cells used for JRODOS calculations for selected NPPs.

1. What is the common impact of individual non-simultaneous radioactive releases in regions with multiple NPPs for a selected area?
2. How can mitigation measures be qualitatively chosen from these common insights?
3. Are these mitigation measures effectively reducing radiation exposure to acceptable limits across all receptors, irrespective of NPP considered?
4. Can a plant-centric software package be applied to a receptor-centric study?

2. Overview of the proposed decision support system

Herein, a DSS is defined as a chain of models/algorithms connected under one information system, following Lim et al. [50]. As such, a DSS aims to perform complex calculations with simpler inputs and step-by-step user-driven decisions to enable quick, accurate, and holistic decision-making. The proposed prototype DSS consists of several modules that work independently, with the information transferred between one or more modules for processing while seamlessly combined under one information framework. Many other DSS follow the same structure, e.g., the IMPAQT DSS [50]. The structure and data flow of the developed

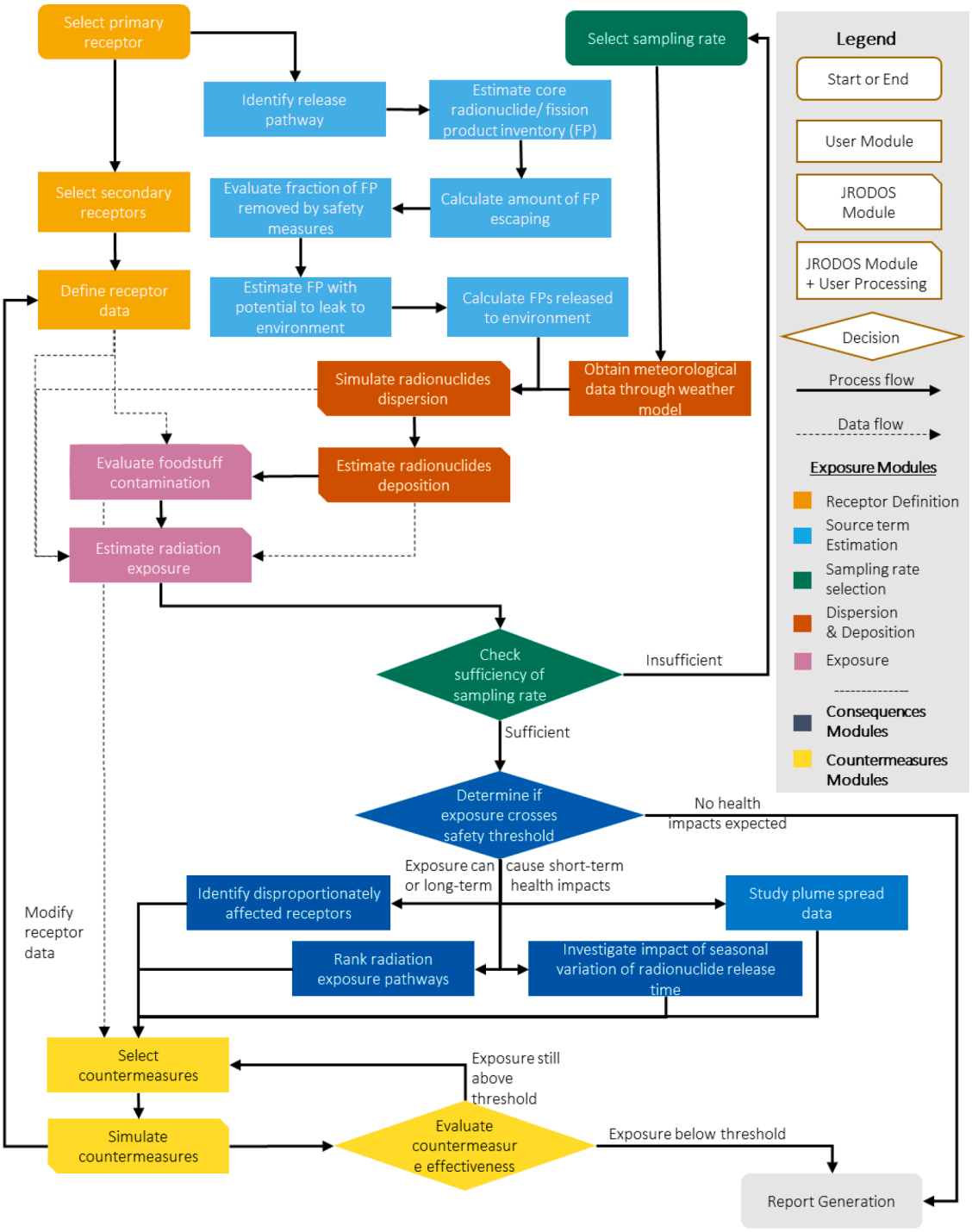

Fig. 2. The flow diagram and modules of the proposed decision support system (DSS) – according to the module owner (shape of blocks) and type of module (color of blocks).

DSS are illustrated in Fig. 2, where each block represents a module of calculations or actions, and each color represents a distinct group of modules. The following paragraph offers a brief overview of the DSS' characteristics. The modules, decision steps, and algorithms are detailed in the following chapters.

In contrast to most of the literature cited earlier, a 'receptor-centric' framework was devised to visualize and analyze the results toward incorporating FEMA's 'community-based planning' recommendation. In this framework, a primary receptor is defined as a unit of analysis that could group several other secondary receptors in the form of other units or subunits. For example, a country could be a primary receptor-unit that consists of multiple other secondary receptor-units such as cities and industries. The latter units can be further split into subunits of districts, communities, and humans. The user will drive the breadth and depth of this discretization to determine the size of the smallest receptor. One of the first rules is that, although, a unit can be inhomogeneous, a subunit should always have apparent homogenous attributes. Thus, there is a greater focus on improving the data associated with every receptor, improving the results' accuracy while accepting the limitations and redundancy of ultra-fine discretization.

Similarly, a 'data-driven' framework was devised to incorporate FEMA's recommendation of considering all hazards during planning. First, this mandated accounting for all the NPPs in the region of interest and deriving shared insights from the impacts of individual non-simultaneous nuclear accidents on a receptor. Second, it required capturing the effect of weather variations and other time-dependent quantities (e.g. atmospheric dispersion, release rate), thus estimating the fate of the radioactive release from each NPP and for different accident start times throughout the year(s). Such a bottom-up approach to consequence assessment facilitates the creation of scalable and flexible ERPs with appropriate plans for each receptor.

3. Exposure assessment methodology

This chapter aims to answer the first question related to understanding the potential impact on a specific region in the presence of multiple NPPs. It starts with a detailed description of the modules related to the impact assessment (Receptors, Source, Dispersion & Deposition, Exposure), following the flow of process and data of the DSS (see Fig. 2), and continues with a discussion on the simulation results.

3.1. Receptors definition and study area

The Middle East is witnessing exponential growth in nuclear power, with Iran, UAE, and KSA spearheading the development of NPPs within the region (Fig. 1). Interestingly, the NPPs in the region surround Qatar, with many closer to Qatar than to the capital cities of the host countries. Thus, Qatar serves as an excellent case study to develop and test a receptor-centric framework. Out of the seven NPP locations, three were considered herein. The Barakah and Bushehr NPPs were chosen because they are the only operational. Umm Huwayd NPP was chosen due to its proximity to Qatar compared to the Darkhovin and Makran Coast NPPs, and its unique position relative to Qatar i.e., West (the others are South-East or North). The other four locations with NPPs were excluded because they are further away, non-operational, or in the vicinity of an included NPP.

The state of Qatar was considered the primary receptor, and it was further subdivided into multiple secondary receptors. These were areas of vital importance to the country, such as cities, transport hubs, industries, desalination plants, oil fields, and gas fields (illustrated in Fig. 1 and enumerated in the SM). The identification and selection process of the secondary receptors (discussed in the SM) was an important step that required significant knowledge, data, and feedback from stakeholders, e.g., population distribution, land use, soil distribution, food consumption habits, inhalation rates, and infrastructure facilities [4]. Ideally, each type of receptor would have its own dataset of characteristics. Due to Qatar being one of the smallest countries, the same uniform food consumption rate, occupancy rate, bathing frequency, and skin covered percentage, among other factors, were used for all receptors. However, for larger and more complex countries and receptors, rigorous and granular data is needed to derive actionable insights. Information on the creation of the dataset for each receptor can be found in the attached supplementary material.

3.2. Source term estimation

Source term estimation is an essential part of studying the impact of any radiological disaster. Any inaccuracies and uncertainties in the source term significantly impact dispersion calculations and subsequent dosage estimations. However, to simplify the computations, many authors have modeled the release with a consistent release rate over the accident duration, sometimes with a limited number of radionuclides [18,21,36]. On the other hand, Mehboob et al. [51] and Jafarikia and Feghhi [52] have shown that radionuclides are not immediately available for release but have a time dependency. Furthermore, the source terms depend on factors such as the reactor type, core inventory, operational reactor history, and accident sequence. Thus, it is essential to use time-dependent source terms specific to the reactor in question to obtain realistic estimates.

As per the US Nuclear Regulatory Commission (NRC) 'NUREG 1228′ Guidelines, the calculation of a source term requires identification of the release pathway. The release pathway is the route along which the radionuclides escape from the core to the atmosphere. For example, the radionuclides can escape through leaks in the suppression pool, bypassing primary containment catastrophic failure, isolation valve failure, or steam generator tube rupture. The release pathway selected herein is the loss of cooling accident (LOCA), one of the most common pathways studied in nuclear safety [53]. According to this pathway, the fission products (FPs) that escape the reactor core are collected within the primary containment. After a 30-minute holdup, the FPs are released to the atmosphere due to either a catastrophic containment failure or an isolation valve failure (100% release). In NUREG 1228 guidelines, both failures lead to an identical release [54].

For each of the employed reactors (more details in the SM), a representative in-containment source term was selected from the works of Mehboob et al. [51] and Jafarikia and Feghhi [52], which considered the molten corium and debris after the accident as the time-dependent source. In brief, Mehboob et al. [51] estimated the core inventory for a generic two-loop 1000 MWe pressurized water reactor (PWR) for LOCA using an in-house code validated against the buildup and decay calculation software ORIGEN 2.1. Similarly, Jafarikia and Feghhi [52]) estimated the Bushehr plant's core inventory using the IRBURNS code, which uses the Monte Carlo MCNP and ORIGEN 2.1 software.

No source term was located in the literature for the Barakah reactor or the APR-1400 model in general, possibly due to this model's limited usage. Only two NPPs in South Korea use this model in addition to Barakah [55]. Consequently, the Mehboob et al. [51] in-containment source term was employed for the Barakah reactor because it is a two-loop PWR [56]. Note that the source term was scaled up by the number of fuel assemblies, assuming their individual fuel assemblies are equivalent.

In the absence of any information about Umm Huwayd's planned reactor, the Jafarikia and Feghhi [52] source term was used for the Umm Huwayd reactor instead of Barakah's source term. The reasons for this were to increase the diversity within the data and, in parallel, enrich the data because the locations of the two reactors are symmetric with respect to the study area (opposite directions and similar distances), which could introduce common artificial patterns in the data.

After obtaining the in-containment source terms for each reactor, these were corrected with release factors from the NRC guidelines to estimate the environmental (released) source-term, using the following assumptions: i) All of the equilibrium radioactive noble gas inventory, at

maximum full power operation of the core, was assumed to be available for leakage from the reactor containment [54]; ii) The iodine released to the environment was split into its components i.e. 91% elemental, 5% particulate, and 4% organic Iodine [57]. The hourly environmental source terms are presented in Fig. 3. Each source was limited to a lower rate threshold of 1E6 Bq/hr, based on screening simulations of the cloud dispersion, which showed no harmful radioactivity levels below this rate around the area of interest. This radioactivity level corresponds to 1 kg of low-level radioactive waste [58]. Finally, the release height was arbitrarily chosen as 50 m for Bushehr and 70 m for Barakah based on the maximum height of each plant's containment dome [52,59]. An intermediate height of 60 m was chosen for Umm Huwayd NPP in the absence of any data.

3.3. Sampling

The date and time of an environmental release are critical as weather fluctuations substantially impact the radioactive cloud spread and the subsequent impact on the receptor. Many studies analyzed real meteorological data and selected days with the highest chance of a worst-case scenario. Some relied on prevailing wind directions alone [36,40]. Others combined wind rose data with precipitation patterns [18,19] and or temperature [41] to select days with worst-case disaster potential. On the other hand, Dvorzhak et al. [23] simulated 8760 accident cases to account for every hour in a full-year meteorological dataset. Clearly, both the worst-case scenario (or arbitrary selection) and every-possible scenario approaches have severe flaws. The former leads to high-impact but low-probability response plans, which may create unnecessarily high economic and social disruption. The latter is computationally intensive and potentially creates a significant amount of noise; especially if it is expanded to more years.

To account for these challenges, Sohrabi et al. [39] used cyclic sampling among meteorological conditions that occur more frequently, and Min and Kim [21] simulated 365 scenarios assuming the release occurs daily at noon. Although the previous two approaches are a compromise between all and just a few meteorological conditions or between fast and intensive computations, they tend to ignore or miss 'black swan events', which are conditions that rarely occur but have potentially severe consequences [61]. Clearly, any sampling technique should be robust to account for weather fluctuations, to create a representative sample of a multi-year dataset at a low computational cost, and to allow the simulation of diverse source terms being released from different NPPs and in multiple years. The more diverse and complete the data is, the more power the decision-maker will have to arrive at an optimum and balanced decision.

In this study, the "stratified random sampling" (SRM) method was tested [62,63] for the generation of simulation scenarios in an arbitrarily selected chronological period, i.e., the year 2017. Following the method's requirements, the chronological period was divided into 365 equal strata (S) of one day. The number of simulations (simulated accidents) per strata -referred to as sampling rate - is an independent and critical parameter of the SRM as it affects the data quality. For example, a small sampling rate may yield an insufficient number of simulated accidents, thus leading to low statistical power and the introduction of unintended biases into the decision-making process. In contrast, a larger sampling rate may yield equivalent sets of scenarios and lead to wasted computational time. To this end, we propose a qualitative decision method (illustrated in Fig. 4) to select the optimum sampling rate, ensuring the representation of frequent and extreme scenarios to the greatest extent possible. To clarify, a simulation refers to a release scenario from one of the NPPs and an estimation of an effective one-year individual dose for each receptor. Eventually, a given sampling rate generates several such simulations and produces a dataset/distribution of one-year individual doses for each receptor. The exploration of the

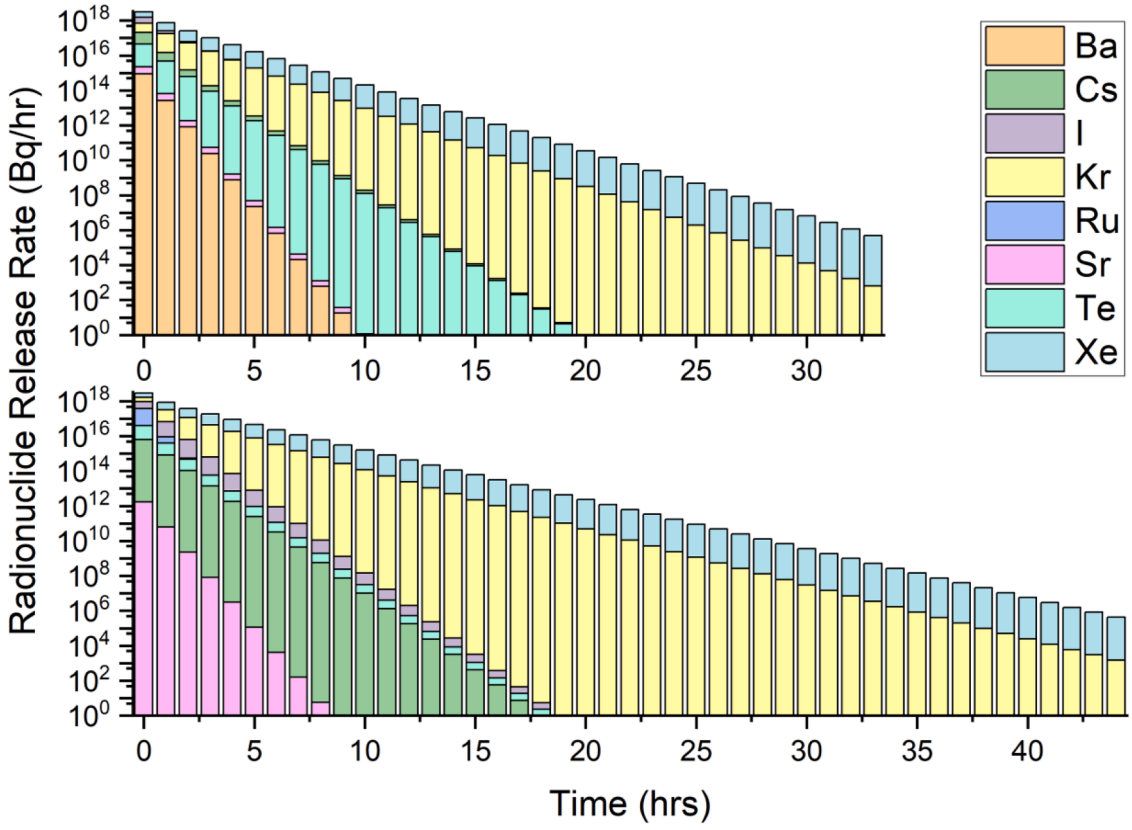

Fig. 3. Top: Hourly environmental source term for Barakah NPP based on Mehboob and Xinrong [60]; Bottom: Hourly environmental source term for Bushehr and Umm Huwayd NPPs based on Jafarikia and Feghhi [52].

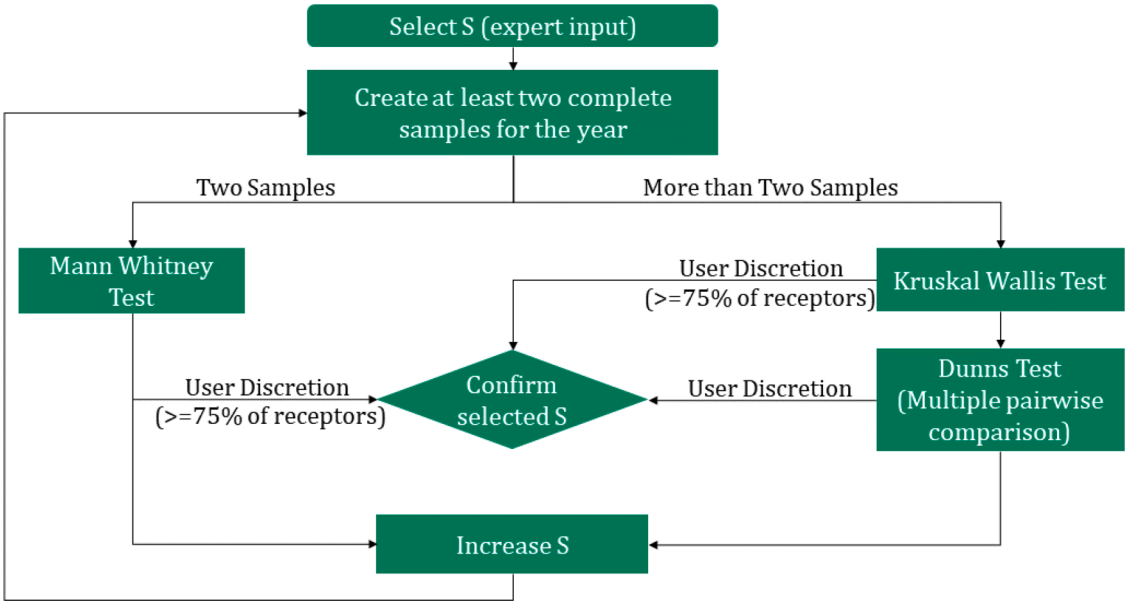

Fig. 4. Proposed qualitative decision method used to select the sampling rate.

optimum sampling rate was guided by assessing the datasets according to the statistical tests in Nayak and Hazra [64].

The proposed method (Fig. 4) starts with selecting a sampling rate, i.e., a number of scenarios to simulate per day (S). At least two complete datasets with this rate are to be created and tested by the below three tests. Since the dose distributions are unknown and the date-dosage pairing is unimportant, the nonparametric tests of the Mann-Whitney U test (2 datasets) and the Kruskal-Wallis tests (>2 datasets) for unpaired data were selected. If the samples are statistically different via the Kruskal-Wallis test, multiple pairwise comparisons using Dunn's test can be performed to see where the difference lies. The Bonferroni correction is suggested for Dunn's test as it is the most commonly used correction in academic articles. All tests were conducted with a confidence level of 95% [64–66]. Herein a cutoff of 25% for all secondary receptors was used for the Mann-Whitney and Kruskal-Wallis tests. In other words, the sampling rate was accepted only if less than 25% of all secondary receptors obtained statistically different dose distributions. For the Dunns test, the pairwise comparison of the distributions can confirm the selection of the sampling rate. For example, when 6 out of 7 datasets showed no statistical difference, the seventh was a possible anomaly and was ignored.

The robustness of the proposed methodology was checked by examining four datasets with a sampling rate of one, and three datasets with a sampling rate of two where no filtering was applied to the datasets. Both sampling rates generated datasets with minimal statistical difference for all NPPs, although the higher sampling rate was marginally better for the Bushehr NPP (4% for sampling rate one, and 0% for two). Barakah & Umm Huwayd NPP showed 0% and 12% difference respectively for both sampling rates. The pairwise comparison using Dunns test showed similar or better results than those in Table 1 and can be found in the SI. Conversely, either sampling rate could be used. Nonetheless, the results with the lower sampling rate were employed hereafter due to its lower computational overhead.

Granted that many past studies employed the simpler wind rose sampling approach, this was also tested and compared to the results obtained from the stratified random sampling approach (presented later).

Table 1
Comparison of samples by Kruskal Wallis test for two sampling rates and all three NPPs with and without dose filtering.

Percentage of receptors with statistically different samples				
	$S = 1$		$S = 2$	
	No Filter	Doses >1 mSv	No Filter	Doses >1 mSv
Barakah	0%	24%	0%	24%
Bushehr	4%	20%	0%	20%
Umm Huwayd	12%	48%	12%	44%

3.4. Atmospheric dispersion and deposition

The JRODOS modules were adopted for dispersion, deposition, food contamination, and dosage calculations. JRODOS was chosen due to its wide adoption in more than 20 institutions across 16 nations in the EU and Asia at national and local levels, lending confidence to its accuracy and versatility [67]. The atmospheric dispersion modeling offers three options: RIMPUFF, DIPCOT, and LASAT [68]. RIMPUFF is a Lagrangian mesoscale puff model [69], while DIPCOT is a Lagrangian particle model [70]. Finally, LASAT is also a Lagrangian particle model with an added diagnostic wind field recommended for use in systems with powerful computational capabilities [71]. However, as the aim was to simulate a large number of cases (>1000) over a simple terrain (Refer to Fig. 1), LASAT was not adopted. Instead, the RIMPUFF model was selected because it performed equally with DIPCOT under simple terrains (as the area of interest) and moderately complex meteorological conditions while being faster [72]. Then, the DEPOM model was employed to calculate the dry and wet depositions [68].

The dispersion and deposition calculations were executed for 72 h for Barakah and 96 h for Bushehr. Initial testing by trial and error showed minimal contribution to Qatar's total gamma dose rate after the periods mentioned above, respectively. Every other dosage calculation was for a one-year time period (more details in later sections).

JRODOS has been designed to study the impact of an NPP incident on the surrounding area and globally. As such, the generated grid is always centered at the NPP with a fixed size or adaptive (finer near the NPP and coarser further away). Consequently, JRODOS provides limited options if one requires a fine spatial resolution for an area of interest further away from the NPP, while avoiding the extensive computational burden of maintaining a high-resolution grid everywhere else. In view of the above, three separate grids were designed for the selected NPPs (Fig. 1), each with four rings and the cell size doubling in every ring (from inside to outside). For the Bushehr NPP, the grid radius was 800 km with a 2 km innermost cell size. For the Barakah and Umm Huwayd NPPs, the

grid radius was 400 km with a 1 km innermost cell size. The effect of the grid size on the results is discussed in a later section.

Numerical weather predictions (NWP) from the NOMADS project of the US NOAA were used to drive the dispersion and deposition calculations in JRODOS. These NWPs cover the global domain, making it easier to simulate accidents from several sources for a primary receptor. The NWP with the finest grid size of 0.5° and smallest temporal resolution (update rate) of 3 h was utilized [73].

3.5. Foodstuff contamination and radiation exposure

The food contamination and radiation exposure were estimated with the Terrestrial Food Chain and Dose Module (FDMT) module from JRODOS (brief description in SM). A key point is that FDMT only calculates the maximum potential contamination, which affects the assessment of the consequences. On the positive side, this would not affect the targeted agricultural countermeasures – more details in the next chapter. The radionuclides considered were iodine (I), cesium (Cs), strontium (Sr), and their isotopes because of their importance [74]. Others, like plutonium (Pu), are of lesser concern, and the FDMT database lacks the requisite data to allow their consideration [75].

Surprisingly, FDMT has two more key assumptions which do not represent the reality in many places worldwide and in Qatar: Food is grown only at the point of consumption and in open-air farms. The issues from the former assumption were bypassed by considering only locally produced food. For a small country like Qatar, the effect of spatial variations of the contamination on the final dosage for each receptor is expected to be small. The latter assumption is more challenging given the large portion of Qatar's food grown in greenhouses [76]. Despite literature showing a significant reduction of contamination in greenhouses due to shielding [14], there is no comprehensive information on the matter. Because the greenhouses across the region use cooling technologies that introduce a large influx of fresh air [77,78], compared to the typical designs in the US and EU [79], and the general lack of data on this topic, the FDMT food contamination results were used without any reduction due to shielding. In addition, the raw dosage was calculated for products that can be sold raw, such as vegetables, fruits, meat, and milk, since the type of processing varies from facility to facility.

For human exposure, radiation dosage to human beings, FDMT accounts for five pathways [75]: i) Inhalation – Cloud & Resuspended radionuclides, ii) Ingestion – Consumption of contaminated food (excluding drinking water), iii) Cloudshine - Radiation from the cloud, iv) Groundshine - Radiation from radionuclides deposited on different surfaces such as the ground, walls, and shrubs, and v) Skin – Radiation from radionuclides deposited on skin and clothes.

The dosages for the ingestion, groundshine and resuspension pathways were estimated for integration times of 7 days, 30 days, 6 months, and 1 year. The dosage for the remaining pathways is only associated with the deposition period, i.e., the duration of the radioactive cloud presence over a receptor. The effective full-body dosage from all nuclides was estimated instead of organ or nuclides-specific doses because such segregation was outside the scope of this work. Similarly, only doses for adults (>18 years) and normal living exposure due to insufficient data for lower age groups and the decision to ignore mitigation measures in the impact assessment. Mitigation and countermeasures are considered in the corresponding chapter. Finally, the collective dose for the residential areas was also estimated for the respective receptors.

4. Consequence assessment results and analysis

The main aim of the consequence assessment modules is to compose the appropriate metrics that reflect the impact of the disaster and feed this information to the countermeasure modules. For example, identifying disproportionately impacted receptors and critical infrastructure (such as desalination plants), as these would need more attention and extra resources to mitigate the impact. Therefore, a semi-qualitative method and the relevant modules (see Fig. 2) were developed around five guiding questions:

1. Are the expected radiation exposures higher than the threshold for either acute short-term or long-term harm?
2. What are the critical exposure pathways of concern for each receptor?
3. Are any receptors disproportionately impacted?
4. Is there a significant seasonality in the exposure depending on the release date/time?
5. What other information can be extracted from cloud spread data (e.g., deployment of an early warning system)?

The following paragraphs describe the methodology and the selected metrics to address one or more guiding questions.

4.1. Total and by pathway effective exposure

The first and most common metric is the level of radiation exposure and whether it exceeds the short-term (acute) and long-term thresholds for health impacts. The thresholds' values vary in the literature, but their exact value does not affect the structure of the proposed DSS. Herein, the 1000 mSv dose for acute radiation syndrome (ARS) was selected as the acute health impact threshold because it is capable of serious health impacts such as radiation burns and nausea. Furthermore, it is likely to cause fatal cancers in 5% of all exposed people [58,80]. The long-term threshold was set to 50 mSv as studies suggest a possible increase in cancer rate in the 50–100 mSv range [80,81]. Dosages below 1 mSv have been filtered out because no health effects are expected at such levels. Hereafter, all dose levels are presented with the use of boxplots and probability density plots. The boxplots illustrate the median value with the upper and lower hinges of the boxes corresponding to the 25th and 75th percentiles and the whiskers covering a range of 1.5 times the interquartile range (IQR) beyond the hinges. The probability density plots were created using kernel density estimation as they use the location of all sample points and capture more information about the population distribution compared to a finite data set [82].

The distribution of the effective individual dose received after a year through the various exposure pathways is visualized in Fig. 5. For all receptors and pathways, more than 75% of the studied scenarios showed no immediate risk of exceeding any of the threshold levels, with the median levels ranging from a few mSv to less than 11 mSv. On the other hand, a significant portion of the estimated dose levels were higher than the long-term health effects threshold (50 mSv) for all receptors. Furthermore, in agricultural areas, cities, desalination plants & gas fields, a few dose levels approached the acute ARS threshold (1000 mSv). Only in oil fields were there levels that crossed the ARS threshold (max ~x4). This analysis illustrates that although not frequent, there is a potential for high-impact radiation incidents.

Among the studied exposure pathways, ingestion was the most critical contributor to individual doses for all secondary receptors. Probably, because it is a recurring source of radioactive dosage in the absence of mitigation. Therefore, the radioactive contamination in different foodstuffs is explored later in the countermeasures chapter. Inhalation was the second biggest contributor to the individual dose, while groundshine was the third one, which happened to be the most critical one for desalination plants. However, either dose seldom crosses the long-term threshold. Indicating that simpler, less disruptive measures to protect the population from non-ingestion doses can be used, and the main focus should be on mitigating the ingestion dose. The remaining two pathways (cloudshine and skin) varied in importance across the receptors. For most receptors, these pathways were not a critical source of radiation exposure. Moreover, the resuspension pathway is missing from Fig. 5, as the highest dose calculated was just 0.016 mSv in the Dukhan oil field area.

The oil field receptors were disproportionately impacted

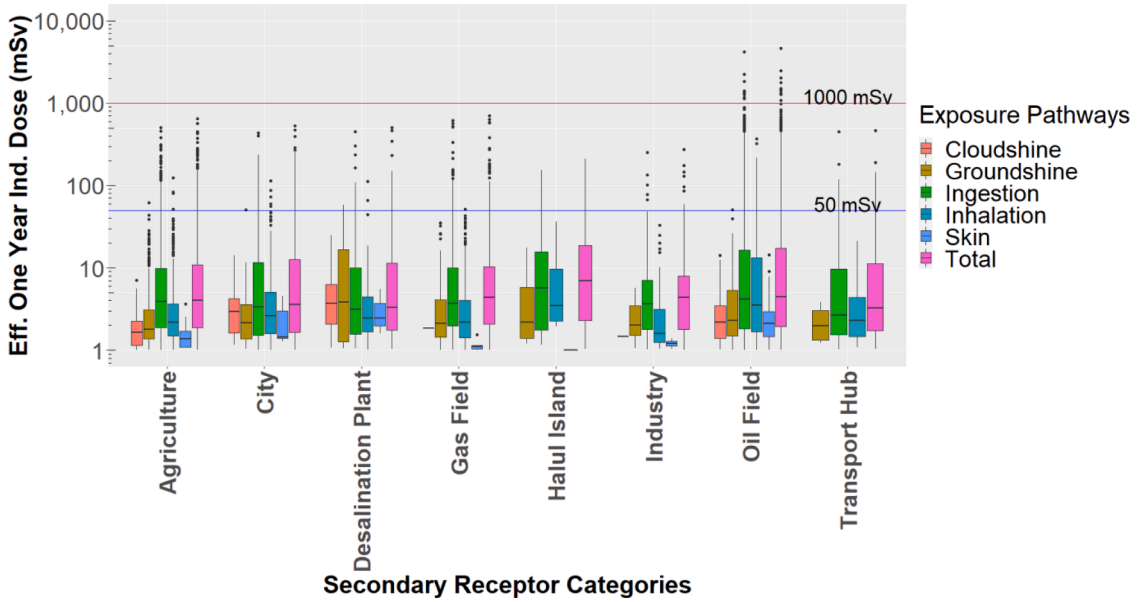

Fig. 5. Box plots of the total and by pathway one-year effective individual doses for the secondary receptor categories (box range corresponds to the 25th and 75th percentiles, and whiskers extend to 1.5x the IQR).

(occasionally exceeding the ARS threshold), for this reason Fig. 6 illustrates the doses for each of the individual receptors within this group. Apparently, only the Dukhan oil field was disproportionately impacted and drove along the whole group, with ingestion being the critical exposure pathway. At this point, it is important to recall that the ingestion pathway represents the exposure through the food produced and consumed in this area. Then again, the Dukhan receptor is further away from most agricultural areas/receptors. Chiefly this observation is misleading and attributed to the FDMT assumption of considering only ingestion at the point of (contaminated) food production rather than allowing for food to be transported from elsewhere. Under these circumstances, the ingestion dose at this oil field would be similar to any other receptor. Whereas, it also indicates that this area is inappropriate for the installation of foodstuff facilities.

In essence, the receptor-centric and robust sampling approach presented herein allowed the identification of critical receptors and pathways and addressed the first three questions posed at the beginning of the chapter.

4.2. *Comparison with wind rose sampling*

Earlier, it was discussed that the use of wind (rose) frequencies is more common in the literature than the simulation of multiple scenarios, regardless of how they are created or sampled. Therefore, this section compares results with the former method against the robust sampling approach proposed herein for one of the region's NPPs, i.e., the Bushehr NPP. Eighteen scenarios were created based on the wind speed and wind directions and aggregated with the frequency of each wind direction sector (Fig. 7a) for the same study period. Only scenarios with wind direction towards Qatar were simulated. Additionally, the scenarios

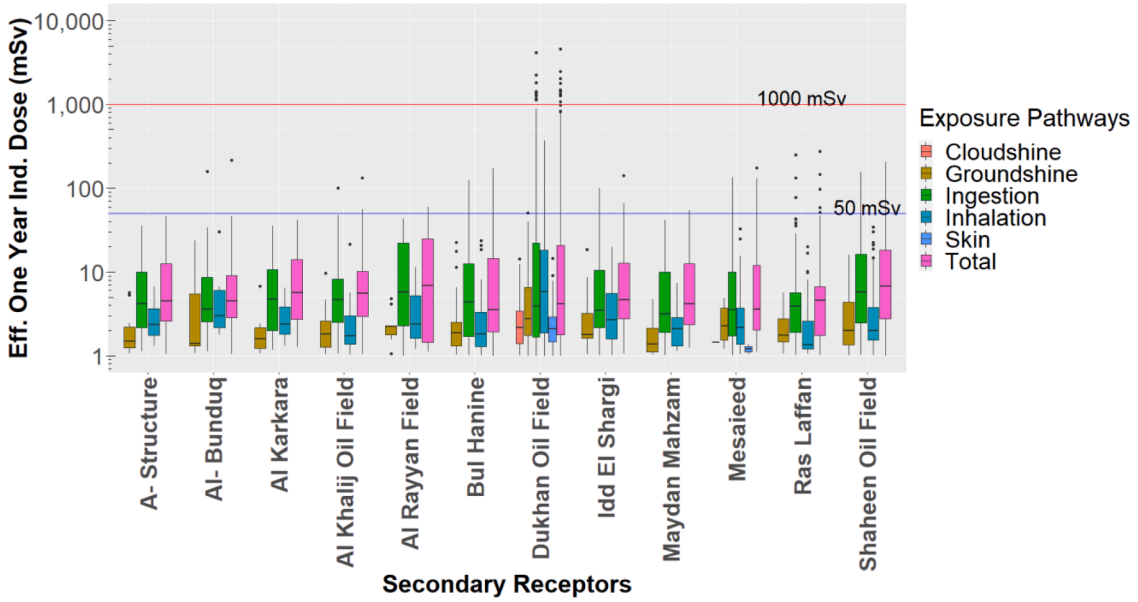

Fig. 6. Effective individual dose received over a year for oil fields and industrial receptors against the acute (red horizontal line) and long-term (blue horizontal line) threshold limits.

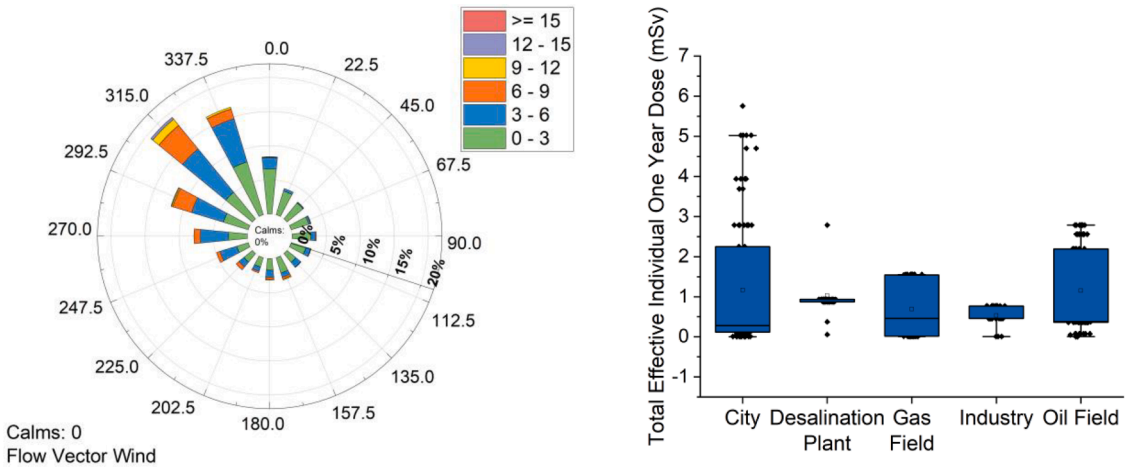

Fig. 7. a) Wind rose and b) Effective one-year individual dose (all doses >0 mSv) from a release at Bushehr NPP obtained from wind rose based sampling.

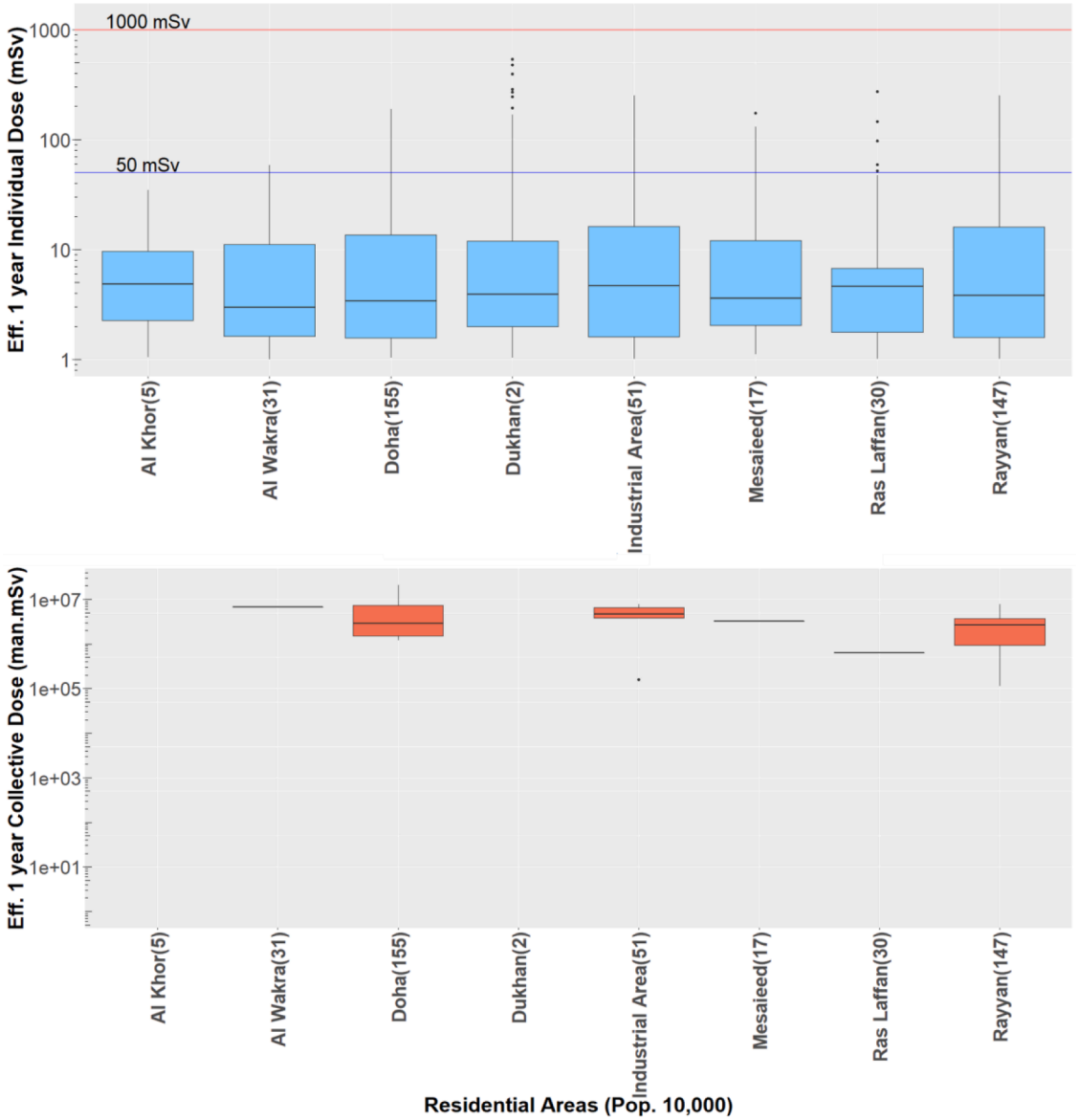

Fig. 8. Effective one year individual (top) & collective (bottom) total dose for residential areas (in parenthesis the population in 10,000ths).

assumed zero precipitation (due to Qatar's exceedingly dry weather), strong insolation for daytime and thin overcast conditions for nighttime, a day duration of 12 h (average between summertime ~14 h and wintertime ~10 h) with sunrise at 6:30 AM. The Pasquil stability classes were estimated accordingly [83]. The scenarios assumed zero precipitation as majority of scenarios expected to have a higher dose (due to higher wind speeds at Bushehr) primarily occurred during the dry summer months. Fig. 7b illustrates the distribution of effective radiation exposure of the different secondary receptors.

The significant underestimation of the doses is obvious when comparing Fig. 7b with Fig. 5. Notably, the wind rose sampling method yielded exposure levels that did not exceed the short- and long-term thresholds at any condition. Furthermore, some secondary receptors showed exposure of less than 1 mSv. Conversely, in our opinion, the wind rose approach cannot support the objectives of a DSS as the one envisioned herein, especially when compared with a robust and expandable sampling methodology.

4.3. Individual vs. collective dose for residential areas

While the individual dose represents the direct impact of radiation to a person, the collective dose is an alternative way to differentiate between different populated areas and prioritize them based on their population density. In other words, this comparison offers the decision makers an additional level for evaluating the actual impact of an accident, or later countermeasure, rather than relying on the typical concentration data and dosage estimations. The concentration or dosage values (i.e. herein individual dosage) may obtain very high values but over an area of little significance for the population i.e. sparsely inhabited. On the other hand, a densely populated area may face large numbers of affected individuals, because of sensitive populations or just of the very large numbers of inhabitants, even at lower levels of concentration and dosage. However, care should be taken while estimating the collective dose to filter out cases with very low individual dose (<50 mSv), since the collective dose may appear high due to a high population density at a given location. In these cases, a high collective dose would not imply any significant health impact on the population. Thus, decision makers should thus use both individual and collective dose in tandem to ensure resources are allocated efficiently and effectively.

Fig. 8 illustrates how the perception of which residential area is affected the most varies significantly between the individual and collective dose methods. For example, Dukhan owned the highest individual dose, but a non-existent collective dose is non-existent due to minimal overlap in areas with doses above the long-term threshold and significant population density . At the same time, a high (or the highest) population density does not automatically lead to the highest collective dose. Despite the fact that Doha has the highest population density, it (alone) does not have the highest collective dose. Conversely, the collective dose would be particularly useful to prioritize receptors, i.e. question three, for both sparsely populated countries (like Qatar) and larger countries with more complex population distributions.

While the individual dose represents the direct impact of radiation to a person, the collective dose is an alternative way to differentiate between different populated areas and prioritize them based on their population density. One such exploration was conducted herein.

4.4. Variation of dosage based on accident start time

The seasonality of the meteorological conditions and of the local climate, i.e. question four, were reflected in the radiation exposure estimates as well. This is presented in Fig. 9 with the probability distribution of the individual dose per season. No special or significant variation dose probability is seen across the seasons in Qatar for the accidents studied . Analysis of the season-to-season and month-to-month variation significantly impacts selecting and implementing appropriate weather countermeasures and planning for special annual events such as pilgrimages and festivals. Especially when one considers that such events inherently have increased attendance, rituals, and restrictions requiring special measures.

4.5. Radioactive cloud trajectory

Finally, the radioactive cloud spread data was qualitatively investigated for additional DSS related metrics (i.e. question five). In particular, the focus was on how it could be used to guide an early warning sensor placement. The effectiveness of an excellent mitigation plan is significantly reduced if not implemented on time, as was the case with the Fukushima Daichi disaster [3].

To this extent, the minimum arrival time of the radioactive cloud for each accident from the different NPPs was considered an appropriate quantity. Specifically, this was arbitrarily measured at grid cells up to a distance of 0.01° outward from Qatar's exclusive economic zone (EEZ)

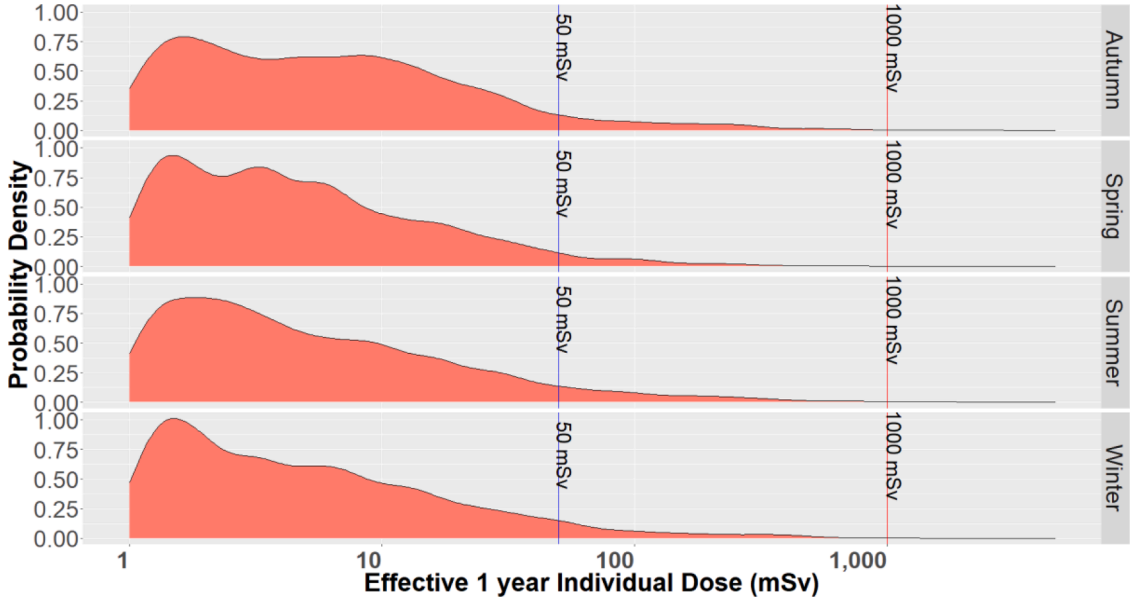

Fig. 9. Seasonal distribution of effective one-year individual dose.

and terrestrial boundaries. Cloud arrival times were defined as the time elapsed between the start of the release and any of the following conditions, according to JRODOS recommendations [84]: i) Time integrated air concentration (nuclide sum) near ground exceeds 1000 Bq s m^{-3}, ii) Total cloud gamma dose rate exceeds 1nSv/h, and iii) Total Ground contamination exceeds 100 Bq m^{-2}.

From Fig. 10, it can be seen that the cloud arrival time varies from as little as one hour to 95 h later, depending on the NPP's distance and the weather conditions. Conversely, the shortest arrival times are for the closest Umm Huwayd NPP (<30 km) and the longest for the farthest Bushehr NPP (~400 km). Despite the quite longer distance of the Bushehr NPP compared to the Barakah NPP (<80 km), they both have similar EEZ arrival times. In addition, the terrestrial arrival times for all three NPPs demonstrate different distribution characteristics attributed to their different locations and weather conditions. Furthermore, there is a clear delay between the cloud reaching the EEZ border and the land borders, which provides an opportunity to detect a radioactive cloud's arrival earlier than reaching the mainland and the majority of the population. A thorough analysis of the arrival times reveals that the Bushehr NPP created a larger percentage of clouds crossing the EEZ border but around half reaching land. This interesting result is due to the EEZ shape, which is wider, close to Bushehr, and narrower on the side of Barakah and Umm Huwayd NPPs. For this reason, leaks from the Umm Huwayd NPP were more than twice as likely to reach Qatar compared to releases from the Barakah NPP. Literature contains different strategies for sea and land-based early waking systems [85].

5. Countermeasure plan

A crucial outcome of a DSS is the selection of countermeasures when an accident occurs. Suitable countermeasures balance the expected public health gain against the possible cost and disruption as recommended by EURANOS for managing nuclear accidents in the EU [86]. After the Chernobyl nuclear accident, many countermeasures were studied and implemented to mitigate the impact of the Chernobyl release [13]. After a brief literature analysis, the following indicative classes of countermeasures were considered hereafter: i) Emergency [86], ii) Agricultural [87–90], iii) Hydrological [91], iv) Urban [86], and v) Medical [92] [Further explained in SM]. Therefore, the chapter starts with the qualitative process of assessing the available countermeasures, according to the DSS' specific modules (see Fig. 2 for reference) before it continues with the details on a few selected countermeasures.

5.1. Selection of countermeasures

One possible way to choose the Emergency countermeasures relates to the minimization of the effective individual 1-year dose while minimizing the economic and social disruptions. Thus, not all countermeasures are appropriate for every situation. For example, emergency countermeasures such as evacuation within a small and flat country like Qatar may not be feasible, while evacuation to an alien neighbor appears a drastic endeavor. On the other hand, sheltering, which used to be considered a complex countermeasure [86], may be easier to implement based on the significant experience with COVID-19 lockdowns [93]. For these reasons, the sheltering countermeasure was selected for demonstration.

The analysis in the previous chapter (e.g. Fig. 5) highlighted the ingestion pathway as the most critical one under the conditions of this study. Thus, agricultural countermeasures were selected to form the core part of the protective strategy. Markedly, many of the related countermeasures, such as plowing and liming soil & crop rotations, were not formulated for greenhouses. Thus, it is impractical to simulate the impact of open-field agricultural countermeasures on greenhouses. Conversely, only food restrictions were explored from agricultural countermeasures, which are feasible since Qatar imports most of its food [94]. Indeed, Qatar has a simplistic food supply chain, and a uniform ingestion dose reduction plan could be employed across all receptors.

No countermeasure was examined from the remaining three classes. In particular, no Urban countermeasure was selected because the groundshine exposure has a minor contribution to the estimated dosages. Medical countermeasures could not be considered in the absence of data for specific radionuclide dosage. Finally, the hydrological countermeasures were not considered, granted that any hydrological related transportation of nuclides was ignored in this version of the DSS.

Important to recall that the selection of countermeasures depends on the conditions of each study, whereas a DSS should be capable of supporting every study. Hence, this chapter serves as a demonstration of the DSS modules and how the metrics and the questions-answers of the previous steps can be utilized.

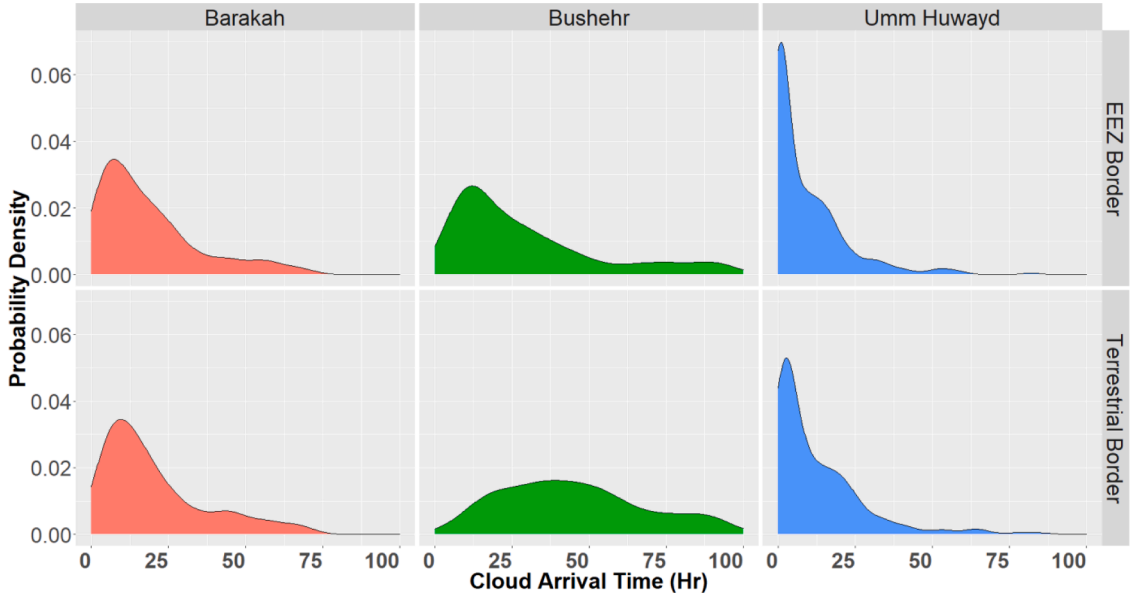

Fig. 10. Cloud arrival time at the EEZ (Top row) and Terrestrial Borders (Bottom row) for accidents at the three NPPs.

5.1.1. Sheltering (Emergency countermeasure)

The sheltering emergency countermeasure is achieved by increasing the indoor occupancy rates i.e., from a mild lockdown to a curfew, for a certain duration, similar to the COVID19 measures implemented in 2021 [95]. The typical occupancy rates for the region are in the order of 90%. Herein a mild lockdown was arbitrarily selected, restricting the time spent outside to half of the day, thus increasing the occupancy rate to 95%. In actuality, the decision makers would need to carry out a cost-benefit analysis to decide which outdoor activities to restrict and accordingly define the occupancy rate. In other words, this countermeasure aims to lower the non-ingestion dose to the population and, conversely, the total dose below the desired threshold. The duration of the sheltering policy can be defined by comparing the approximated dosage over fixed periods.

Fig. 11 illustrates the variation of the radiation exposure (non-ingestion, ingestion, and total dose) for seven days and one year integration times for all secondary receptors. Nearly all the non-ingestion radiation exposure occurs in the first seven days, with the ingestion dose driving the radiation exposure for the remaining period. Thus, the implementation of sheltering toward a 95% occupancy rate for the first seven days after the incident could eliminate most of the non-ingestion dose. Moreover, this data reveals that an immediate decision and response are critical to mitigate the ingested dose, with any delay reducing the effectiveness of the countermeasure exponentially.

5.1.2. Food restrictions (agricultural countermeasure)

The significant contribution of the ingestion dose to the total dose became clear in the previous countermeasure (Fig. 11). Therefore, it is essential to identify which foods to be restricted and for how long. At the same time, it is impossible to restrict all foods. Therefore, the proposed DSS methodology aims to restrict just enough foods to drop the exposure below the earlier thresholds. Furthermore, this countermeasure can be implemented by either restricting a food's consumption or replacing its source with a non-contaminated one until the successful decontamination of the cultivation and production facilities. Note that neither the cost of such a countermeasure nor the duration of the decontamination of the food production areas was explored. Nevertheless, for demonstration reasons, a one-year duration was selected.

The guideline level (GL) for food contamination after a nuclear accident proposed by the Joint FAO/WHO Codex Alimentarius Commission was used to guide food restrictions. The guideline level GL (Bq/kg) is the maximum level of allowable contamination in food, above which governments need to decide whether to allow this food in their territory. Therefore, the lowest guideline values for isotopes of I, Cs, and Sr present in the source term, were calculated (Values in SM). The lowest GL for each radionuclide was selected for a conservative estimate, i.e., 681, 788, and 535 Bq/kg, respectively. The typical formulation of GL levels is shown in Eq. (1) [96].

$$GL = \frac{E}{M \times e_{ing} \times F} \quad \text{(Eq. 1)}$$

Where

GL	is the guideline level (Bq/kg)
E	is the allowable annual effective individual dose (mSv)
M	is the age-dependent food consumption rate (kg)
e_{ing}	is the age-dependent ingestion dose coefficient (mSv/Bq)
F	is the contamination fraction

Herein, the E was set at one mSv based on the IAEA recommendation [96]. The ingestion dose coefficients from the International Commission on Radiological Protection (ICRP) were used for e_{ing} [97]. For the product MxF, the sum of the contaminable food consumption data was required. As Qatar imports a significant amount of its foodstuff, only food grown within Qatar was considered to be contaminated. It is expected that Qatar will modify its supply chain as needed to ensure all imported food is uncontaminated (further explained in SM).

The food contamination levels (CL) for the different foodstuff from JRODOS have been plotted in Fig. 12 against the smaller GL of 535 Bq/kg (Sr Isotope) for visual clarity since all GLs are close.

Nearly all foods cross the GL. Leafy vegetables especially show disproportionately high contamination levels, likely due to their larger surface area compared to other foods. In contrast, lamb and chicken do not show high contamination levels. FDMT calculates only the iodine contamination of lamb, but similar results are expected for the other isotopes. Following this approach (depicted in Fig. 12), the DSS would have suggested restricting all foods except lamb and chicken. However, this is not feasible, as it would cause considerable disruptions. For this reason, another method was explored to visualize the contamination data and aid decision-making while accounting for the GL. Accordingly, the normalization of the GL with the CL was selected (Eq. (2)) to create a single 'food restriction metric' (FRM) from which one can graphically

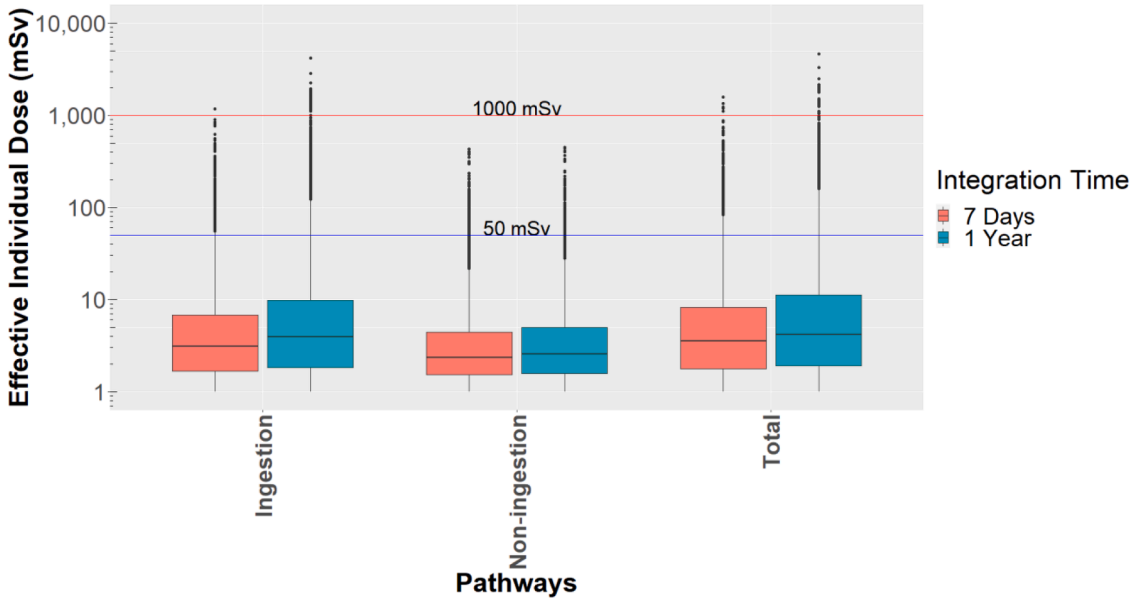

Fig. 11. Integrated radiation exposure by various pathways seven days and one year after the accident against the acute (red horizontal line) and long-term (blue horizontal line) threshold limits.

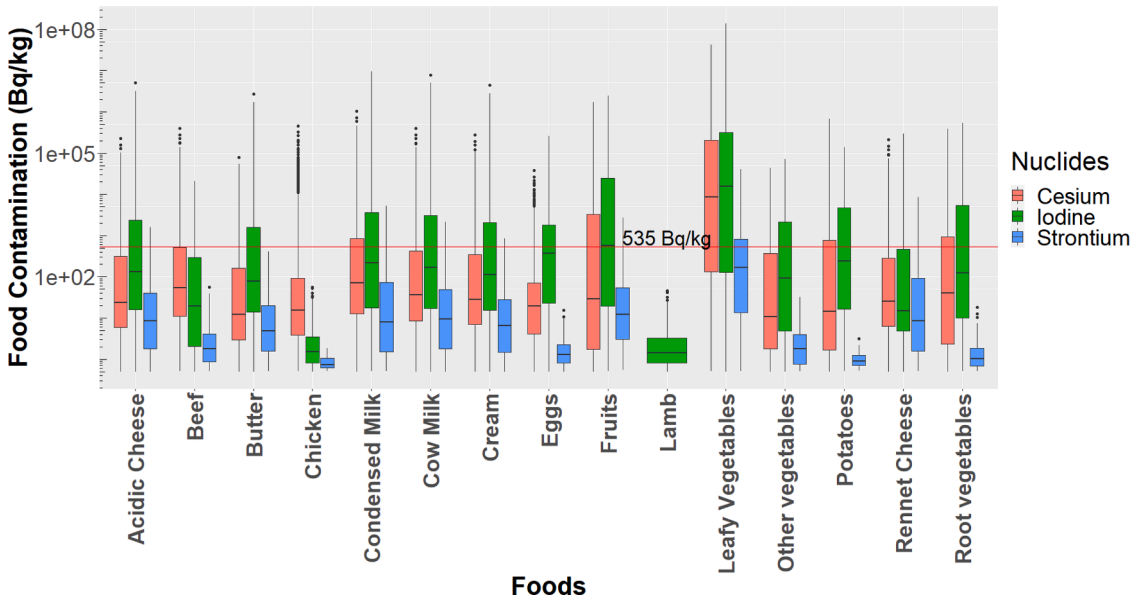

Fig. 12. Box plots of the cesium, iodine and strontium contamination levels (CL) of foodstuffs against the I guideline levels (GL; red horizontal line).

select which foods to restrict. In other words, foods with high FRM value should be prioritized.

$$FRM = \frac{GL}{CL} \quad \text{(Eq. 2)}$$

Because the CL levels vary (see Fig. 12), the median was used. Alternatively, contamination values at higher percentiles or even the maximum contamination could be used based on user discretion.

The FRM rankings for all isotopes are visualized in Fig. 13, with significant differences among the three isotopes. By examining different scenarios, the restriction of four foods with the highest FRM for each nuclide was arbitrarily selected. The foods to be restricted would be leafy vegetables, condensed milk, cow milk, beef, eggs, and rennet cheese, accounting for 47% of the daily food consumption rate by weight.

Note that the above method uses the original calculation of CL which does not utilize the available food-wise consumption data but uses a lumped food consumption rate in FxM (in Eq. (1)). A new FRM based on each food's respective consumption rates was tested, hereafter referred to as the individual FRM method. The ranking based on the individual FRM is shown in Fig. 14, which pointed to the restriction of leafy vegetables, cow milk, condensed milk, cream, beef, and rennet cheese - accounting for 45% of the daily food consumption rate by weight. Although both methods point to nearly identical food restrictions, the user can select restrictions based on additional criteria. Here, we opted for the latter method of the individual FRM (as in Fig. 14) because it

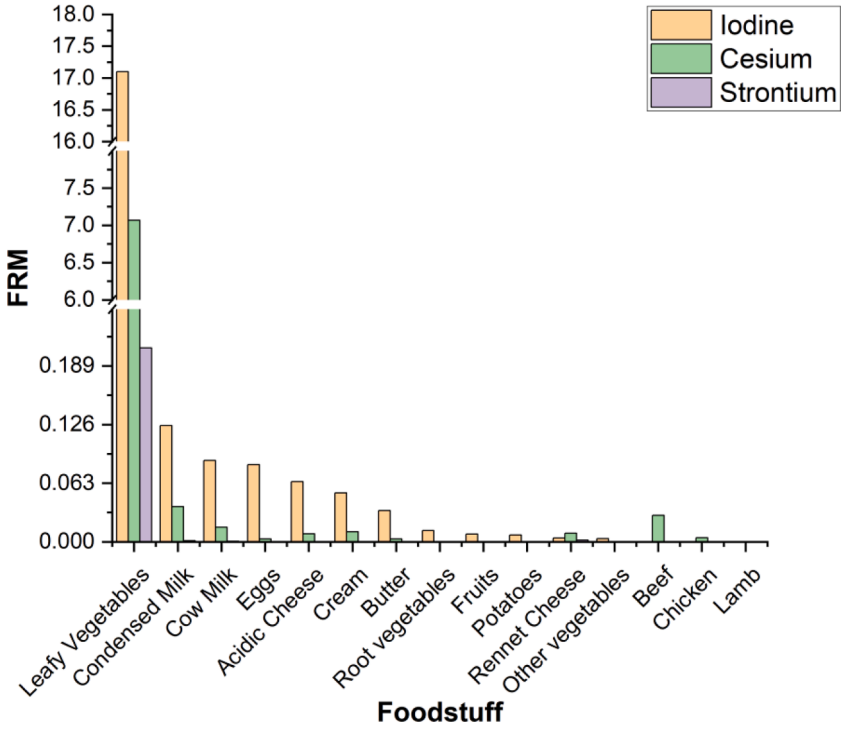

Fig. 13. Lumped food restriction metric (FRM) for I, Cs and Sr radionuclides.

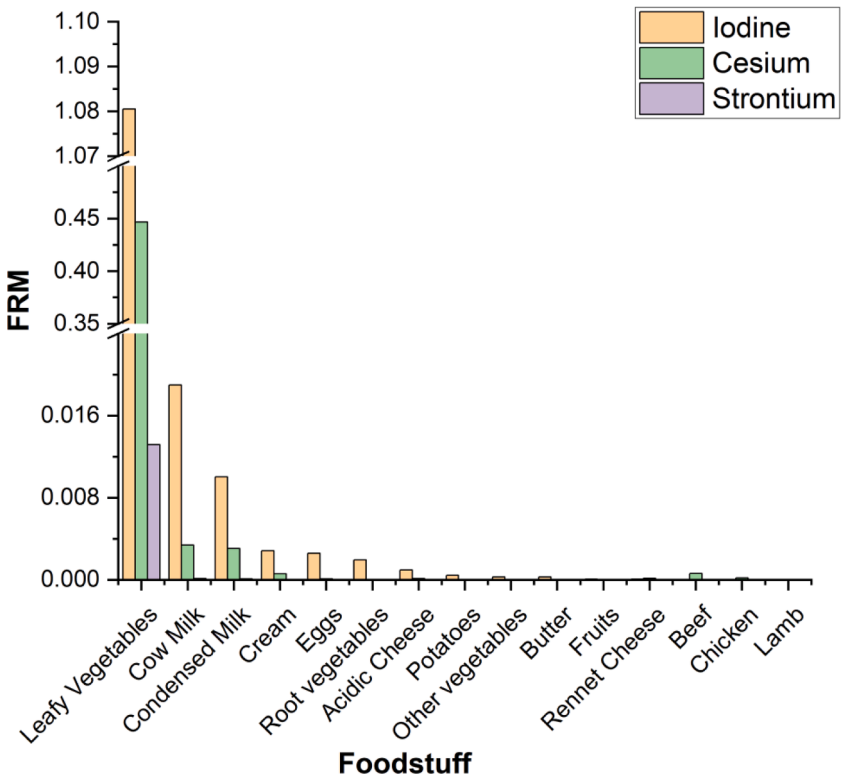

Fig. 14. Individual food restriction metric (FRM) for I, Cs and Sr radionuclides.

identifies more clearly the top three food than the lumped FRM (as in Fig. 13), which shows smaller differences among the second to fifth-ranked foods.

5.2. *Effect of countermeasures*

For most receptors, sheltering reduces the median and highest values of the non-ingestion dose (Fig. 15), indicating a possibly successful countermeasure. However, the drop is significantly lesser than expected given the restrictions applied. Moreover, for some receptors, like the Industry and Desalination Plants, the median value and/or the quantiles' extent (box size) increase compared to without sheltering. The inherent statistical variation, driven by the sampling of data, and the small population of the receptors were considered the main reasons for this complication. In all cases, the sheltering period and scale appear inadequate to bring the extremes below the long-term threshold limit requiring more strict measures.

Similar conclusions are extracted from the food restrictions after a comparison of the ingestion doses with and without this countermeasure (Fig. 16), with most receptors achieving lower median and extreme levels. Again, for the same receptors, i.e., Industry and Desalination Plants, the quantiles' range and/ or the medians increased, while the

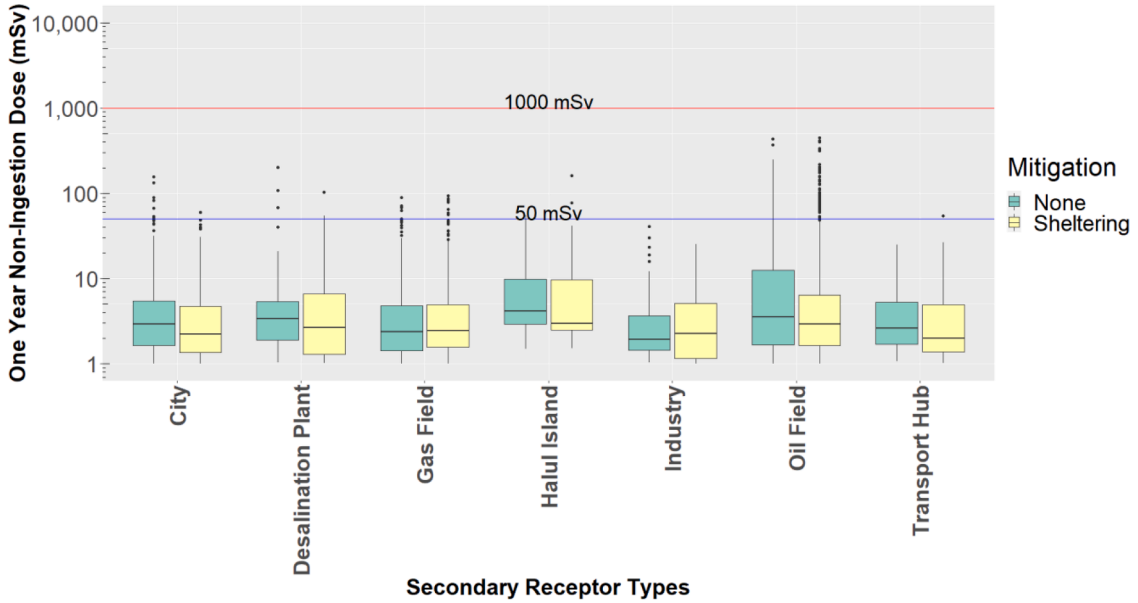

Fig. 15. Non-ingestion dose with and without Sheltering compared against the acute (red horizontal line) and long-term (blue horizontal line) threshold limits.

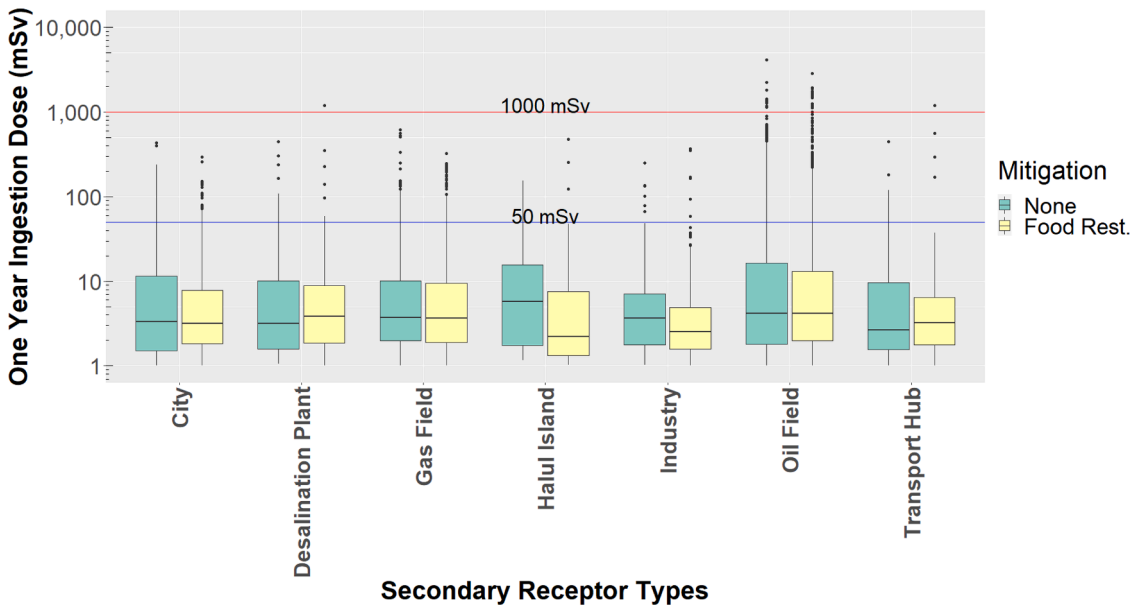

Fig. 16. Ingestion Dose with and without Food Restrictions against the acute (red horizontal line) and long-term (blue horizontal line) threshold limits.

effect of the countermeasures were much lower than expected for the significant amount of food restrictions suggesting need for stricter countermeasures.

The anomalous behavior in both cases suggests an insufficient sampling rate questioning the proposed sampling rate selection method's validity. This deficiency of the sampling rate selection method could be due to the significant amount of noise in the datasets. As, on average, 98% of values in the dataset are 0 or close to it, the unfiltered datasets appear statistically similar. However, in this study, the non-zero dosages, particularly the ones above 1 mSv, are of interest.

Thus, to check the sampling method to our region of interest, the method was applied to the datasets but for only doses above 1 mSv, similar to filtering done in the above plots with results in Table 1 below.

Table 1 shows that filtering the doses results in very different results where essentially the proposed sampling rates are not sufficient for Barakah and Umm Huwayd NPP and barely sufficient for Barakah NPP. This result explains the variation seen in Fig. 15& Fig. 16. Filtering to higher doses would similarly only result in a greater variation. Thus, a much higher sampling rate is needed for the current combination of receptors, NPPs, and accident scenarios. However, this study could not simulate higher sampling rates due to the high computational overhead of using a plant-centric grid to a receptor-centric grid, suggesting that plant-centric software is not appropriate for a receptor-centric study.

6. Conclusions and areas of improvement

A prototype DSS framework for evaluating the impact of accidents from nuclear plants and prioritizing countermeasures was created based on a novel receptor-centric framework based on FEMA guidelines. One of the main new aspects was analyzing the impact of non-simultaneous individual accidents in regions with multiple NPPs and how to obtain actionable insights toward a mitigation strategy. The framework is also data-driven, thus suggesting the stratified random sampling (SRM) to consider, generate, and consolidate scenarios with all possible consequences i.e., negligible, mild, and severe consequences. A methodology for selecting an optimal accident sampling rate within the SRM was proposed while keeping the computational efforts low. Although the SRM was shown to be superior against simpler approaches like the worst-case meteorology or the wind rose sampling, more data is still needed to accept or reject the utility of this method conclusively. Possible use of trajectory analysis from the NPP to simplify the SRM process also remains an area of study. The importance of filtering the datasets to only include regions of concern was demonstrated along with the impact of an insufficient sampling rate on the results' quality.

In the core of the DSS lies the JRODOS which was successfully tested for the State of Qatar for accidents from three out of the five nearby nuclear power plants. However, many aspects of the present JRODOS did not allow for full exploitation of the receptor-centric and data-driven framework presented herein. These include the grid type for exposure calculations, the FDMT assumptions on food production and consumption, and the randomizer algorithm's parameterization. In particular, the calculation grid controls not only the resolution of the dispersion modules but the input data processing as well. Fig. 17 shows a direct comparison of the land-use data mapped on the generated grids for the three studied power plants and one with the main receptor at the grid origin, even though this last case was not simulated. The amount of lost information is profound, with large portions of the urban area missing and narrow sea insertions replaced by desert. Of course, fine grid resolution does not necessarily translate to improvement. The FDMT, at its current version, enforces the food consumption, and production happening only within the same grid cell, with obvious implications. Although in this work, the large grid cells and the small size of Qatar reduced the undesired granulation in the food contamination calculations, future versions should account for local and regional supply chains.

Despite that it was out of the scope of this work, several other aspects were tested to assess the sensitivity and uncertainty of employed assumptions based on literature approaches (e.g. [98,99]). Probably, the one worth mentioning most after the grid-generation is a qualitative comparison of the dispersion estimations of the RIMPUFF and DIPCOT models. Fig. 18 illustrates the effective gamma dose 96 h after a selected release scenario. The differences in the results are clear, although the hot areas agree. RIMPUFF produced higher levels and a seemingly problematic cloud spread with large discontinuous areas while DIPCOT produced a smoother dispersion across all affected areas. Note that both tools used the exact same input. The different patterns, can be attributed to the fundamentally different approaches in the two models (puffs vs. particles respectively) and how they are affected by rapid weather changes [69]. The above concerns a single scenario but clearly, the components of the proposed framework require further testing and validation. Nonetheless, this work highlighted the insights that a fully functional receptor-centric and data-driven DSS framework can offer to

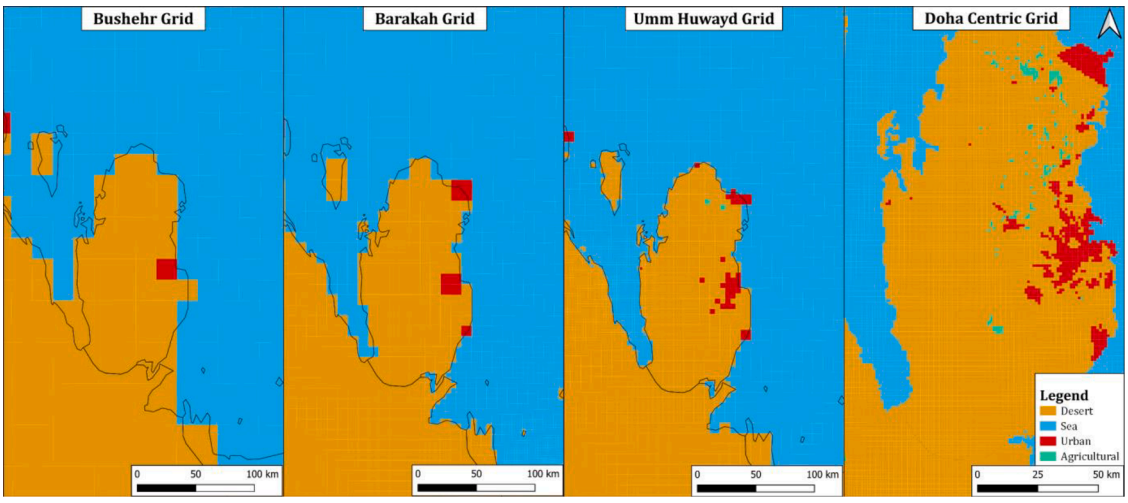

Fig. 17. Land use maps used within JRODOS for the generated grids for each of the studies power plants, and one with the main receptor (city of Doha) at the grid's origin.

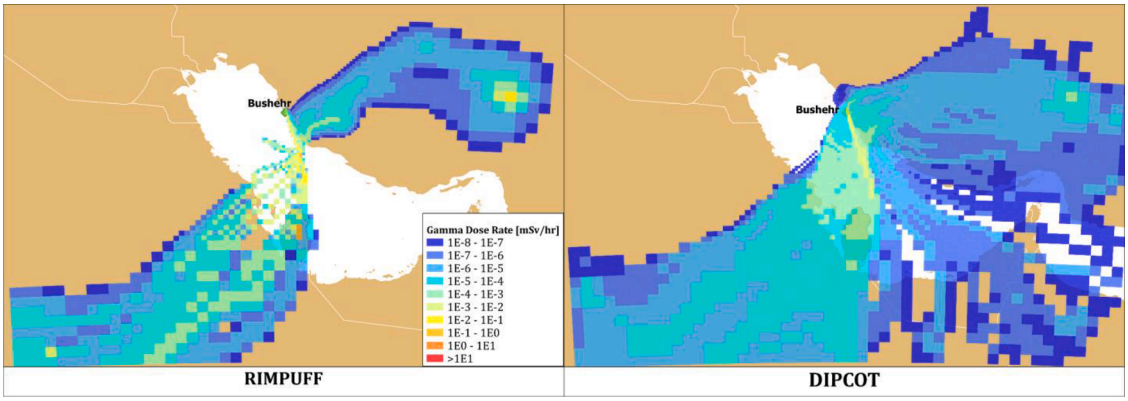

Fig. 18. Comparison of the total effective gamma dose for RIMPUFF & DIPCOT at the 96th hour of simulation after hypothetical release from Bushehr on 18th July 2017.

the effective planning and real-time response for nuclear accidents.

Concerning the introduced questions, this work outlined one of the first decision support systems, with specific examples, on combining the impact assessment of multiple nuclear power plants into one framework. Further, it provided evidence that this framework can deduce critical mitigation measures by analyzing the exposure pathways and dosages at the receptor level. On the other hand, the examined methods of synthesizing the produced data proved to be less sensitive to variations of the suggested measures and, conversely, not adequate to conclude the most appropriate one. Regardless, the suggested measures were adequate overall to reduce direct and indirect exposure to radiation.

CRediT authorship contribution statement

Arshad Mohamed Ali: Conceptualization, Methodology, Software, Data curation, Writing – original draft, Visualization. **Konstantinos E Kakosimos:** Conceptualization, Methodology, Writing – review & editing, Supervision, Project administration.

Declaration of Competing Interest

The authors declare the following financial interests/personal relationships which may be considered as potential competing interests: Arshad Mohammed Ali reports financial support was provided by Qatar National Research Fund.

Data availability

I have shared a link to a data repository Processed Simulation Data used in generating tables and figures in Manuscript (Original data) (GitHub)

Acknowledgments

This publication was made possible by a GSRA award [GSRA6-2-0612-19081] from the Qatar National Research Fund (a member of Qatar Foundation). The contents herein are solely the responsibility of the authors. Open Access funding provided by Qatar National Library. The authors would like to thank Karlsruhe Institute of Technology (KIT)/JRODOS team for providing the software and their help in its installation.

Supplementary materials

Supplementary material associated with this article can be found, in the online version, at doi:10.1016/j.ress.2023.109474.

References

[1] Datablog. Nuclear power plant accidents: listed and ranked since 1952. The Guardian; 2011.

[2] LAKA Foundation. IAEA-database of nuclear and radiological incidents.
[3] Funabashi Y, Kitazawa K. Fukushima in review: a complex disaster, a disastrous response. Bull Atom Sci 2012;68:9–21.
[4] FEMA. Developing and maintaining emergency operations plans. 2010.
[5] Al-Douri A, Levine CS, Groth KM. Identifying human failure events (HFEs) for external hazard probabilistic risk assessment. Reliab Eng Syst Saf 2023;235:109236.
[6] Kim Y, Jang S, Jae M. Evaluation of inter-unit dependency effect on site core damage frequency: internal and seismic event. Reliab Eng Syst Saf 2022;227:108748.
[7] Laboratory LLN. History (of NARAC).
[8] Nasstrom JS, Sugiyama G, Baskett RL, Larsen SC, Bradley MM. The National Atmospheric Release Advisory Center modelling and decision-support system for radiological and nuclear emergency preparedness and response. Int J Emergency Manage 2007;4.
[9] Ievdin I, Trybushny D, Zheleznyak M, Raskob W. RODOS re-engineering: aims and implementation details. Radioprotection 2010;45.
[10] Chino M, Ishikawa H, Yamazawa H. SPEEDI and WSPEEDI: Japanese emergency response systems to predict radiological impacts in local and workplace areas due to a nuclear accident. Radiat Prot Dosim 1993;50:145–52.
[11] Raja Shekhar SS, Venkata Srinivas C, Rakesh PT, Deepu R, Prasada Rao PVV, Baskaran R, et al. Online Nuclear Emergency Response System (ONERS) for consequence assessment and decision support in the early phase of nuclear accidents - Simulations for postulated events and methodology validation. Prog Nucl Energy 2020;119.
[12] Fesenko S, Jacob P, Ulanovsky A, Chupov A, Bogdevitch I, Sanzharova NI, et al. Justification of remediation strategies in the long term after the Chernobyl accident. J Environ Radioact 2010;119.
[13] Kirichenko VA, Kirichenko AV, Werts DE. Consequences and countermeasures in a nuclear power accident: Chernobyl experience. Biosecur Bioterror 2012;10:314–20.
[14] Zehringer M. Radioactivity in food: experiences of the food control authority of basel-city since the chernobyl accident. 2016.
[15] Lin W, Chen L, Yu W, Ma H, Zeng Z, Zeng S. Radioactive source terms for the Fukushima nuclear accident. Sci China Earth Sci 2015;59:214–22.
[16] Helton JC, Johnson JD, Shiver AW, Sprung JL. Uncertainty and sensitivity analysis of early exposure results with the MACCS reactor accident consequence model. Reliab Eng Syst Saf 1995;48:91–127.
[17] Ytre-Eide M, Standring W, Amundsen I, Sickel M, Liland A, Saltbones J, et al. Consequences in Norway of a hypothetical accident at Sellafield: potential release – transport and fallout. 2009.
[18] Liland A, Lind OC, Bartnicki J, Brown JE, Dyve JE, Iosjpe M, et al. Using a chain of models to predict health and environmental impacts in Norway from a hypothetical nuclear accident at the Sellafield site. J Environ Radioact 2020;214-215:106159.
[19] Aliyu AS, Ramli AT, Saleh MA. Environmental impact assessment of a new nuclear power plant (NPP) based on atmospheric dispersion modeling. Stoch Environ Res Risk Assess 2014;28:1897–911.
[20] Aliyu AS, Ramli AT, Saleh MA. Assessment of potential human health and environmental impacts of a nuclear power plant (NPP) based on atmospheric dispersion modeling. Atmósfera 2015;28:13–26.
[21] Min JS, Kim HR. Environmental impact on the Korean peninsula due to hypothetical accidental scenarios at the Haiyang nuclear power plant in China. Prog Nucl Energy 2018;105:254–62.
[22] Tang Z, Cai J, Li Q, Zhao J, Li X, Yang Y. The regional scale atmospheric dispersion analysis and environmental radiation impacts assessment for the hypothetical accident in Haiyang nuclear power plant. Prog Nucl Energy 2020;125.
[23] Dvorzhak A, Mora JC, Robles B. Probabilistic risk assessment from potential exposures to the public applied for innovative nuclear installations. Reliab Eng Syst Saf 2016;152:176–86.
[24] Cho J, Lee SH, Bang YS, Lee S, Park SY. Exhaustive simulation approach for severe accident risk in nuclear power plants: OPR-1000 full-power internal events. Reliab Eng Syst Saf 2022;225:108580.
[25] Mazgaj P, Darnowski P, Kaszko A, Hortal J, Dusic M, Mendizábal R, et al. Demonstration of the E-BEPU methodology for SL-LOCA in a Gen-III PWR reactor. Reliab Eng Syst Saf 2022;226:108707.
[26] Di Maio F, Matteo F, Guerini C, Federico P, Zio E. Time-dependent reliability analysis of the reactor building of a nuclear power plant for accounting of its aging and degradation. Reliab Eng Syst Saf 2021:205.
[27] Guo Z, Dailey R, Feng T, Zhou Y, Sun Z, Corradini ML, et al. Uncertainty analysis of ATF Cr-coated-Zircaloy on BWR in-vessel accident progression during a station blackout. Reliab Eng Syst Saf 2021;213:107770.
[28] Cho J, Han SH. Identification of risk-significant components in nuclear power plants to reduce Cs-137 radioactive risk. Reliab Eng Syst Saf 2021;211.
[29] Queral C, Gómez-Magán J, París C, Rivas-Lewicky J, Sánchez-Perea M, Gil J, et al. Dynamic event trees without success criteria for full spectrum LOCA sequences applying the integrated safety assessment (ISA) methodology. Reliab Eng Syst Saf 2018;171:152–68.
[30] París C, Queral C, Mula J, Gómez-Magán J, Sánchez-Perea M, Meléndez E, et al. Quantitative risk reduction by means of recovery strategies. Reliab Eng Syst Saf 2019;182:13–32.
[31] Rebollo MJ, Queral C, Jimenez G, Gomez-Magan J, Meléndez E, Sanchez-Perea M. Evaluation of the offsite dose contribution to the global risk in a Steam Generator Tube Rupture scenario. Reliab Eng Syst Saf 2016;147:32–48.
[32] Song W, Park S, Seo Y, Jae M. A source term binning methodology for multi-unit consequence analyses. Reliab Eng Syst Saf 2020;202.
[33] Jang S, Kim Y, Jae M. A site risk assessment for internal events: a case study. Reliab Eng Syst Saf 2021;215:107876.
[34] Francesco DM, Matteo F, Carlo G, Federico P, Enrico Z. Time-dependent reliability analysis of the reactor building of a nuclear power plant for accounting of its aging and degradation. Reliab Eng Syst Saf 2021;205:107173.
[35] Ebel ER. Geopolitics of the iranian nuclear energy program: but oil and gas still matter (CSIS reports). Center for Strategic & International Studies; 2010.
[36] Pirouzmand A, Dehghani P, Hadad K, Nematollahi M. Dose assessment of radionuclides dispersion from Bushehr nuclear power plant stack under normal operation and accident conditions. Int J Hydrogen Energy 2015;40:15198–205.
[37] Sohrabi M, Parsouzi Z, Amrollahi R, Khamooshy C, Ghasemi M. Public exposure from environmental release of radioactive material under normal operation of unit-1 Bushehr nuclear power plant. Ann Nucl Eng 2013;55:351–8.
[38] Raisali G, Davilu H, Haghighishad A, Khodadadi R, Sabet M. Calculation of total effective dose equivalent and collective dose in the event of a LOCA in Bushehr Nuclear Power Plant. Radiat Prot Dosimetry 2006;121:382–90.
[39] Sohrabi M, Ghasemi M, Amrollahi R, Khamooshi C, Parsouzi Z. Assessment of environmental public exposure from a hypothetical nuclear accident for Unit-1 Bushehr nuclear power plant. Radiat Environ Biophys 2013;52:235–44.
[40] Beeley PA, Kim S-Y. Preliminary radioactive dispersion modeling in the Arabian gulf using the ADMS-5 Gaussian plume model. peaceful use of nuclear energy and its impact on environmental security. Bahrain: Royal College of Bahrain Police; 2014.
[41] Mohammed Saeed IM, Saleh MAM, Hashim S, Hama YMS, Hamza K, Al-Shatri SH. The radiological assessment, hazard evaluation, and spatial distribution for a hypothetical nuclear power plant accident at Baiji potential site. Environ Sci Eur 2020;32.
[42] Gyamfi K, Birikorang SA, Ampomah-Amoako E, Fletcher JJ. Radiological safety analysis for a hypothetical accident of a generic VVER-1000 nuclear power plant. Sci Technol Nucl Installat 2020;2020:1–8.
[43] Poon CB, Au SM, Prohl G, Muller H. Adaptation of ecosys-87 to Hong Kong Environmental Conditions. Health Phys 1997;72:856–64.
[44] Li JX, Cao XW, Tong LL, Huang GF. Radiological consequence evaluation of DBAs with alternative source term method for a Chinese PWR. Nucl Eng Des 2012;250:260–6.
[45] Shamsuddin SD, Koh MH, Basri NA, Omar N, Koh M-H, Ramli AT, et al. Radioactive dispersion analysis for hypothetical nuclear power plant (NPP) candidate site in Perak state, Malaysia. In: EPJ Web of Conferences. 156; 2017.
[46] World Nuclear Association. Nuclear power in iran. World Nuclear Association; 2020.
[47] Johnson S. Middle east countries plan to add nuclear to their generation mix. US Energy Information Administration; 2018.
[48] Brumfiel G. As saudi arabia builds a nuclear reactor, some worry about its motives. NPR; 2019.
[49] Yoo H, Heo G. Analysis of site operating state contributions for multi-unit PSA with Korean NPP Sites. Reliab Eng Syst Saf 2023;236:109274.
[50] Lim LL, Hughes SJ, Hellawell EE. Integrated decision support system for urban air quality assessment. Environ Model Softw 2005;20:947–54.
[51] Mehboob K, Park K, Khan R. Quantification of in-containment fission products source term for 1000 MWe PWR under loss of coolant accident. Ann Nucl Eng 2015;75:365–76.
[52] Jafarikia S, Feghhi SAH. Study of in-containment source term behavior for VVER-1000 under LOCA conditions using the IRBURN code system. Ann Nucl Eng 2018;112:17–29.
[53] Joyce M. Chapter 14 - Nuclear Safety and Regulation. editor. In: Joyce M, editor. Nuclear engineering. Butterworth-Heinemann; 2018. p. 323–55.
[54] McKenna T.J., Glitter J.G. Source term estimation during incident response to severe nuclear power plant accidents. Washington, DC1988.
[55] KEPCO. APR1400. KEPCO.
[56] UAE Federal Authority for Nuclear Regulation. Safety evaluation report of an application for a licence to construct barakah units 1 and 2. Abu Dhabhi: FANR; 2012.
[57] Soffer L., Burson S.B., Ferrell C.M., Lee R.Y., Ridgely J.N. Accident source terms for light-water nuclear power plants. Washington, DC1995.
[58] World Nuclear Association. Nuclear radiation and health effects. 2020.
[59] Emirates Nuclear Energy Corporation. Final dome structure completed at Barakah nuclear energy plant. 2018.
[60] Mehboob K, Xinrong C. Source term evaluation of two loop PWR under hypothetical severe accidents. Ann Nucl Eng 2012;50:271–84.
[61] Taleb NN. The black swan: the impact of the highly improbable. Penguin; 2007.
[62] Hankin DG, Mohr MS, Newman KB. Sampling theory: for the ecological and natural resource sciences. Oxford, UNITED KINGDOM: Oxford University Press USA - OSO; 2019.
[63] Powers AB. Stratified random sampling. 4th ed. Springer Publishing Company; 2010.
[64] Nayak BK, Hazra A. How to choose the right statistical test? Indian J Ophthalmol 2011;59:85–6.
[65] Dinno A. Nonparametric pairwise multiple comparisons in independent groups using Dunn's test. Stata J 2015;15:292–300.
[66] Marusteri M, Bacarea V. Comparing groups for statistical differences: how to choose the right statistical test?. 2009.
[67] Wengert A. JRodos: an off-site emergency management system for nuclear accidents. Karlsruhe Institute of Technology (KIT); 2017.
[68] Ievdin I, Trybushnyi D, Landman C, Staudt C. JRodos user guide V4.0 2019.
[69] Thykier-Nielsen S, Deme S, Mikkelsen T. Description of the atmospheric dispersion module. RIMPUFF; 1999.

[70] Andronopoulos S, Davakis E, Bartzis JG. RODOS-DIPCOT model description and evaluation. 2002.
[71] Raskob W., Landman C., Trybushnyi D. JRODOS: real-time online decision support system for nuclear emergency management. Karlsruhe Institute of Technology.
[72] Päsler-Sauer J. Comparison and validation exercises of the three atmospheric dispersion models in RODOS. Radioprotection 2010;45:S89–96.
[73] NOAA. Global forecast system (GFS). NOAA.
[74] WHO, FAO. Nuclear accidents and radioactive contamination of foods. 2011.
[75] Müller H, Gering F, Pröhl G. Model description of the terrestrial food chain and dose module FDMT in RODOS PV6.0 RODOS. GSF - Institut für Strahlenschutz; 2003.
[76] Burdon-Manley L. Qatari farmers trying to find new ways to increase production. Al Jazeera; 2017.
[77] Al-Mulla Y. Cooling Greenhouses in the Arabian Peninsula. Acta Hortic 2006;719:499–506.
[78] Alkhalidi A, Khawaja MK. Abusubaih D. Energy efficient cooling and heating of aquaponics facilities based on regional climate. Int J Low Carbon Technol 2020;15:287–98.
[79] Karanisa T, Amato A, Richer R, Abdul Majid S, Skelhorn C, Sayadi S. Agricultural production in Qatar's hot arid climate. Sustainability 2021;13.
[80] WHO. Ionizing radiation, health effects and protective measures. 2016.
[81] Vaiserman A, Koliada A, Zabuga O, Socol Y. Health impacts of low-dose ionizing radiation: current scientific debates and regulatory issues. Dose-Response 2018;16:1559325818796331.
[82] Weglarczyk S. Kernel density estimation and its application. In: ITM Web of Conferences; 2018. p. 23.
[83] Pasquill F. The estimation of the dispersion of windborne material. The Meteorological Magazine; 1961. p. 33–49.
[84] Ievdin I, Landman C, Päsler-Sauer J, Staudt C. Result guide for the models in the JRODOS emergency model chain V3.0. 2019.
[85] Dombrowski H, Bleher M, Cort MD, Dabrowski R, Neumaier S, Stöohlker U. Recommendations to harmonize European early warning dosimetry network systems. J Instrum 2017;12:P12024. -P.
[86] Brown J, Mortimer K, Andersson KG, Duranova T, Mrskova A, Hänninen R, et al. Generic handbook for assisting in the management of contaminated inhabited areas in europe following a radiological emergency. Didcot: Health Protection Agency; 2007.
[87] Alexakhin RM. Countermeasures in agricultural production as an effective means of mitigating the radiological consequences of the Chernobyl accident. Sci Total Environ 1993;137:9–20.
[88] Segal MG. Agricultural countermeasures following deposition of radioactivity after a nuclear accident. Sci Total Environ 1993;137:31–48.
[89] Shinano T. Mitigation of radioactive contamination from farmland environment and agricultural products. Mod Environ Sci Eng 2016;2:454–61.
[90] IAEA, FAO. Strategies and Practices in the Remediation of Radioactive Contamination in Agriculture: Report of a Technical Workshop in Vienna, Austria, 17–18 October 2016. Vienna: IAEA; 2020.
[91] Smith JT, Voitsekhovitch OV, Håkanson L, Hilton J. A critical review of measures to reduce radioactive doses from drinking water and consumption of freshwater foodstuffs. J Environ Radioact 2001;56:11–32.
[92] Arora R, Chawla R, Marwah R, Kumar V, Goel R, Arora P, et al. Medical radiation countermeasures for nuclear and radiological emergencies: current status and future perspectives. J Pharm Bioallied Sci 2010;2:202–12.
[93] FT Visual & Data Journalism Team. Lockdowns compared: tracking governments' coronavirus responses. Financial Times; 2021.
[94] Planning & Statistics Authority. Agricultural statistics. Doha; 2017.
[95] Al Jazeera. Qatar announces new restrictions amid fears of second covid wave. Al Jazeera; 2021.
[96] IAEA. Criteria for radionuclide activity concentrations for food and drinking water. Vienna; 2016.
[97] Eckerman K, Harrison J, Menzel HG, Clement CH. ICRP publication 119: compendium of dose coefficients based on ICRP publication 60. In: Annals of the ICRP. 42; 2013.
[98] Sanchez-Saez F, Sánchez AI, Villanueva JF, Carlos S, Martorell S. Uncertainty analysis of a large break loss of coolant accident in a pressurized water reactor using non-parametric methods. Reliab Eng Syst Saf 2018;174:19–28.
[99] Cooke R. Uncertainty in dispersion and deposition in accident consequence modeling assessed with performance-based expert judgment. Reliab Eng Syst Saf 1994;45:35–46.